

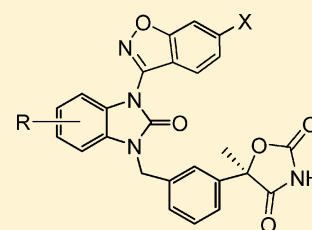
Benzimidazolones: A New Class of Selective Peroxisome Proliferator-Activated Receptor  $\gamma$  (PPAR $\gamma$ ) Modulators<sup>†</sup>

Weiguo Liu,\* Fiona Lau, Kun Liu, Harold B. Wood, Gaochao Zhou, Yuli Chen, Ying Li, Taro E. Akiyama, Gino Castriota, Monica Einstein, Chualin Wang, Margaret E. McCann, Thomas W. Doebber, Margaret Wu, Ching H. Chang, Lesley McNamara, Brian McKeever, Ralph T. Mosley, Joel P. Berger, and Peter T. Meinke

Merck Research Laboratories, P.O. Box 2000, Rahway, New Jersey 07065, United States

## Supporting Information

**ABSTRACT:** A series of benzimidazolone carboxylic acids and oxazolidinediones were designed and synthesized in search of selective PPAR $\gamma$  modulators (SPPAR $\gamma$ Ms) as potential therapeutic agents for the treatment of type II diabetes mellitus (T2DM) with improved safety profiles relative to rosiglitazone and pioglitazone, the currently marketed PPAR $\gamma$  full agonist drugs. Structure–activity relationships of these potent and highly selective SPPAR $\gamma$ Ms were studied with a focus on their unique profiles as partial agonists or modulators. A variety of methods, such as X-ray crystallographic analysis, PPAR $\gamma$  transactivation coactivator profiling, gene expression profiling, and mutagenesis studies, were employed to reveal the differential interactions of these new analogues with PPAR $\gamma$  receptor in comparison to full agonists. In rodent models of T2DM, benzimidazolone analogues such as (5*R*)-5-(3-([3-(5-methoxybenzoxazol-3-yl)benzimidazol-1-yl]methyl)phenyl)-5-methyloxazolidinedione (**51**) demonstrated efficacy equivalent to that of rosiglitazone. Side effects, such as fluid retention and heart weight gain associated with PPAR $\gamma$  full agonists, were diminished with **51** in comparison to rosiglitazone based on studies in two independent animal models.



## INTRODUCTION

Diabetes is a metabolic disorder escalating in the world population at an alarming rate.<sup>1</sup> Non-insulin-dependent type 2 diabetes mellitus (T2DM) accounts for more than 90% of the cases. It is characterized by insulin resistance in the liver and peripheral tissues. To achieve the physiologically required level of glucose metabolism, diabetic patients require more insulin by either increased endogenous production or direct injection of the recombinant peptide. Both processes disrupt the normal functioning of the insulin producing organ and often result in pancreatic  $\beta$ -cell dysfunction. One way to tackle the underlying causes for T2DM would be to increase the sensitivity of tissues and therefore the body's response to insulin.

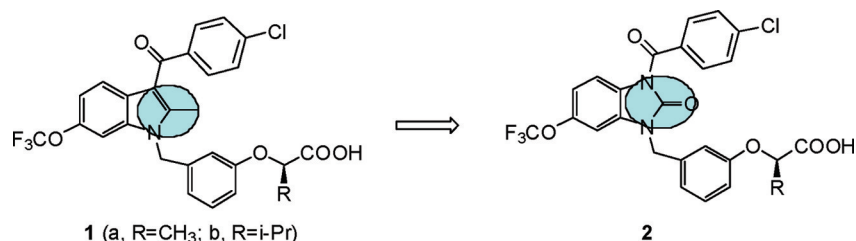
The peroxisome proliferator-activated receptors (PPARs) comprise a subfamily of ligand-activated nuclear hormone receptors<sup>2</sup> that are involved in regulating nutrient storage and catabolism.<sup>3</sup> There are three PPAR subtypes, commonly designated as PPAR $\alpha$ , PPAR $\gamma$ , and PPAR $\delta$ ( $\beta$ ).<sup>4</sup> Agonists of the  $\gamma$  subtype have been studied extensively for their role in regulating glucose metabolism and insulin sensitivity.<sup>5</sup> PPAR $\gamma$  full agonists, such as rosiglitazone and pioglitazone, have been developed and marketed for the treatment of T2DM.<sup>6</sup> However, mechanism-based side effects including weight gain, edema, congestive heart failure, and the recently reported increased risk for bone fracture following rosiglitazone or pioglitazone treatment are major untoward effects associated with the use of PPAR $\gamma$  full agonists.<sup>7,8</sup> Lately, several reports in the literature,<sup>9</sup> including work from our own laboratories,<sup>10</sup>

have demonstrated that selective PPAR $\gamma$  modulators (SPPAR $\gamma$ Ms) bind to their receptors in a distinct mode relative to full agonists, providing a physical basis for differential pharmacological effects. Such ligands act as partial agonists in cell-based transcriptional activity assays and induce an attenuated adipocyte gene signature. In preclinical species, SPPAR $\gamma$ Ms were shown to retain antidiabetic efficacy comparable to that of full PPAR $\gamma$  agonists while displaying reduced PPAR $\gamma$  mechanism-based adverse effects.<sup>11</sup> Recently, we reported the discovery of a series of indole-based carboxylic acids. These selective PPAR $\gamma$  modulators<sup>12</sup> showed potent PPAR $\gamma$  activity in binding assays, partial agonism in cell-based transactivation assays, and robust effects in lowering hyperglycemia in rodent models of diabetes. While pursuing the SARs of this series of analogues, we discovered that the indole core structures could be replaced by benzimidazolones, resulting in increased selectivity toward PPAR $\gamma$  receptors and a unique interaction profile with a panel of PPAR coactivators. In this report, we describe X-ray crystallographic analyses, mutagenesis studies, and coactivator recruiting patterns of this new class of benzimidazolone SPPAR $\gamma$ Ms, as well as their SARs and in vivo antidiabetic efficacy vs propensity to induce side effects in preclinical species.

Received: August 7, 2011

Published: November 9, 2011

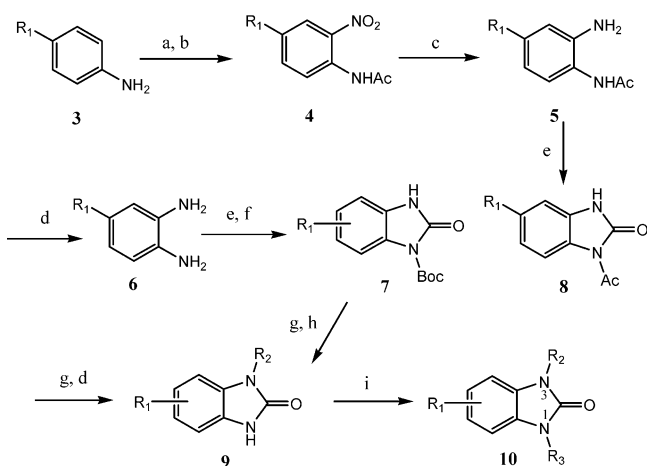
Chart 1. Benzylindole Carboxylic Acid vs Benzimidazolone Carboxylic Acid



## CHEMISTRY

In the previous reports,<sup>12c</sup> we described a series of *N*-benzylindole carboxylic acid analogues (**1**, Chart 1) as SPPAR $\gamma$ Ms. Although potent, this class of compounds suffered a few drawbacks such as modest inhibition in a panel of cytochrome P450 enzymes, multiple off-target hits in a commercial in vitro screen of common enzymes and receptors (Panlabs), and some residual PPAR $\alpha$  activity which complicates interpretation of efficacy results.<sup>10b</sup> Conversion of the indole core into an azaindole decreased the number of off-target hits and P450 inhibition. However, these azaindole analogues suffered from poor PK characteristics and thus diminished in vivo efficacy.<sup>13</sup> In the context of expanding SAR and improving properties, we sought to replace the indole with a non-indole moiety while retaining the overall structural topology and the general SAR trend. The benzimidazolone design (**2**) fits this criteria and allows the introduction of substitutions at both imidazolone nitrogens, mimicking the 1,3-indole substitution. A series of such 1,3-disubstituted benzimidazolone analogues were prepared following procedures as depicted in Scheme 1.

### Scheme 1<sup>a</sup>



<sup>a</sup>Reagents and conditions: (a) AcOH/Ac<sub>2</sub>O, 0 °C; (b) AcOH/HNO<sub>3</sub>, room temp; (c) Pd/C/H<sub>2</sub>, MeOH; (d) NaOH, MeOH; (e) CDI, THF; (f) NaH/(Boc)<sub>2</sub>O, followed by column separation of two regioisomers; (g) R<sub>2</sub>-Cl/Cs<sub>2</sub>CO<sub>3</sub>/DMF, R<sub>2</sub> = benzisoxazole, benzothiazole, acyl, or benzyl; R<sub>2</sub>-B(OH)<sub>2</sub>, dppe/Pd(OAc)<sub>2</sub>/dioxane, R<sub>2</sub> = Ar; (h) TFA/MeOH; (i) R<sub>3</sub>-Br, Cs<sub>2</sub>CO<sub>3</sub>/DMF, room temp.

Starting from properly substituted anilines (**3**) or phenylenediamines (**6**), protected benzimidazolone cores were prepared by routine chemical manipulations. The acetyl protected benzimidazolones (**8**) with position of R<sub>1</sub> clearly defined were initially used for subsequent transformations. However, the acetyl group was labile under many alkylation conditions, which often

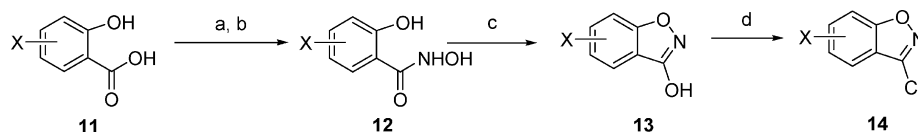
resulted in double alkylation products and poor yields. Boc protection was later found to be more stable for *N*-alkylation and was commonly used for scale-up chemistry. The two regioisomers resulting from Boc protection were separated by flash chromatography and confirmed by comparison with products derived from **8**. The first *N*-substitution by acylation, alkylation, or boronic acid coupling followed by deprotection gave intermediate **9** with diverse R<sub>2</sub> groups. Introduction of a variety of R<sub>3</sub> bearing acidic moieties as the second *N*-substitution affords a targeted combinatorial library of benzimidazolones analogues (**10**).

Several key R<sub>2</sub> and R<sub>3</sub> moieties were prepared as depicted in Schemes 2–4. Starting with properly substituted salicylic acids (**11**), esterification followed by treatment with hydroxylamine gave the corresponding hydroxamates (**12**). Cyclization with carbodiimide followed by heating with phosphorus oxychloride gave the substituted 3-chlorobenzisoxazoles (**14**).<sup>14</sup> The chiral phenoxycarboxylic acids or esters were prepared following procedures as described in previous reports.<sup>12c</sup> Mitsunobu coupling between a substituted anisole (**15**) and a chiral ethyl lactate (**16**) followed by free radical bromination yielded the desired benzyl bromides (**18**). Synthesis of the chiral oxazolidinedione moieties involved multistep chemical and asymmetric transformations as shown in Scheme 4. Again, starting with a properly substituted anisole, formation of the trifluoromethanesulfonyl ester (OTf) with subsequent palladium (dppp) catalyzed coupling using vinyl butyl ether gave intermediate **19**<sup>15</sup> which was hydrolyzed in HCl to yield the acetophenone (**20**). Wittig reaction of the acetophenone gave the corresponding  $\alpha$ -methylstyrene (**21**) which was subjected to Sharpless's asymmetric dihydroxylation conditions to produce the corresponding chiral diols (**22**).<sup>16</sup> Oxidation of this diol with Pt/C followed by esterification with diazomethane afforded the carboxylic ester (**24**). Cyclization of the  $\alpha$ -hydroxycarboxylic ester with urea in sodium ethoxide produced the chiral oxazolidinedione (**25**), which was protected by a trityl group followed by bromination with NBS and AIBN in carbon tetrachloride to give the benzyl bromide moiety (**27**) ready for attachment to the benzimidazole core as the R<sub>3</sub> substitution.

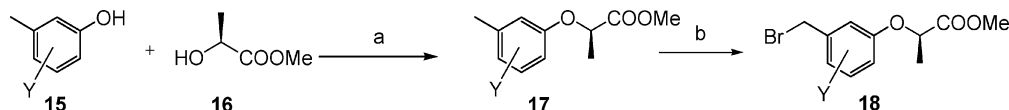
Systematic variation of R<sub>1</sub>, R<sub>2</sub>, and R<sub>3</sub> groups in conjunction with a convergent assembly process led to the syntheses of large numbers of benzimidazolone analogues (**10**). In this communication, only selected examples of these compounds are presented to illustrate SAR.

## RESULTS AND DISCUSSION

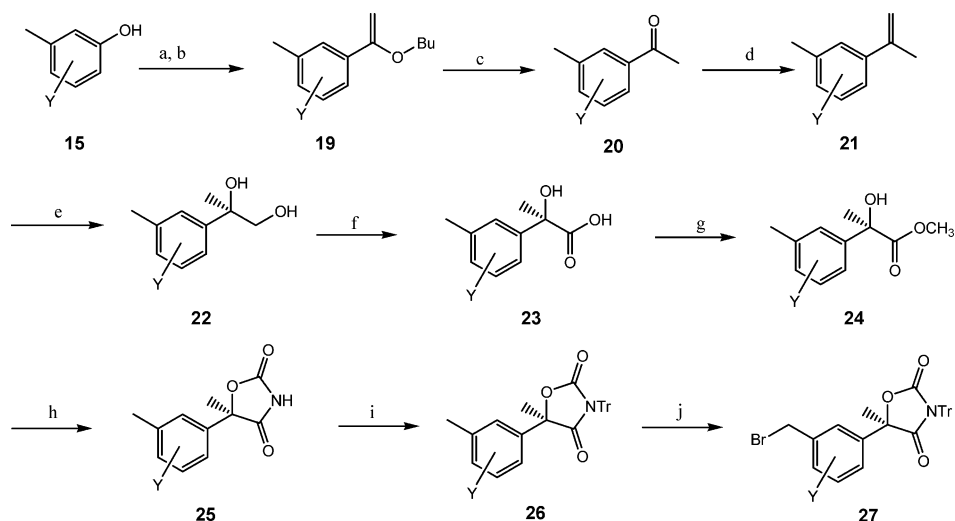
In several previous reports, we have described extensive SAR studies of indole-<sup>12</sup> and azaindole-containing<sup>13</sup> SPPAR $\gamma$ Ms. For the benzimidazolone series, our initial efforts were to compare their PPAR $\gamma$  activity with similar analogues in the indole series. Although retaining their binding affinity, selectivity, and partial

Scheme 2<sup>a</sup>

<sup>a</sup>Reagents and conditions: (a) TMS-CH<sub>2</sub>N<sub>2</sub>, benzene/MeOH (4:1), room temp; (b) NH<sub>2</sub>OH, NaOH, dioxane, room temp; (c) CDI/THF, 75 °C; (d) POCl<sub>3</sub>, Et<sub>3</sub>N, 90 °C.

Scheme 3<sup>a</sup>

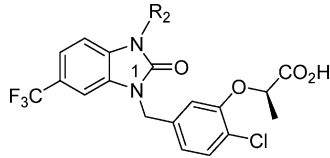
<sup>a</sup>Reagents and conditions: (a) PPh<sub>3</sub>/DIAD, CH<sub>2</sub>Cl<sub>2</sub>, room temp; (b) NBS/AIBN, CCl<sub>4</sub>, reflux.

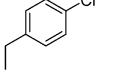
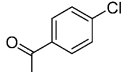
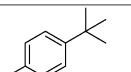
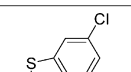
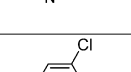
Scheme 4<sup>a</sup>

<sup>a</sup>Reagents and conditions: (a) Tf<sub>2</sub>O/Py; (b) vinyl butyl ether, dppp/NEt<sub>3</sub>/Pd(OAc)<sub>2</sub>, DMF, 80 °C; (c) HCl, MeOH; (d) Ph<sub>3</sub>PCH<sub>3</sub>Br/*n*-BuLi, ether; (e) AD-mix β, <sup>t</sup>BuOH/H<sub>2</sub>O, 0 °C; (f) 10% Pt/C, NaHCO<sub>3</sub>, H<sub>2</sub>O, 70 °C; (g) CH<sub>2</sub>N<sub>2</sub>, Et<sub>2</sub>O; (h) urea/NaOEt, EtOH, reflux; (i) TrCl/Et<sub>3</sub>N, CH<sub>2</sub>Cl<sub>2</sub>; (j) NBS/AIBN, CCl<sub>4</sub>, reflux.

agonist activity, these new SPPAR $\gamma$ M<sub>s</sub> exhibited divergent SAR and certain unique profiles. The selected analogues described herein are summarized in Tables 1–7. Their biological activities are evaluated on two criteria: their affinity for human PPAR $\gamma$  and PPAR $\alpha$  (IC<sub>50</sub>)<sup>17</sup> and their agonist activity in a human PPAR-GAL4 transactivation assay in COS-1 cells in terms of potency (EC<sub>50</sub>) and maximum activation (Max) relative to rosiglitazone for PPAR $\gamma$  agonism.<sup>10</sup> Initial SAR was focused on systematic variations of R<sub>2</sub> with constant R<sub>1</sub> and R<sub>3</sub> substitutions (Table 1). Direct analogues of the most potent agonists in the indole series such as 28 and 29 were only moderately active. The *tert*-butylphenyl substituted analogue 30 showed good binding activity. However, activation level was very low in the transactivation assay. The benzisoxazole substitution as R<sub>2</sub> yielded the most potent analogue (32), with a 68 nM binding potency and a typical partial agonist profile in the transactivation assay. Next, the effects of different substitutions on the benzisoxazoles (Table 2) were examined. In general, most types and positions of substitution on the benzisoxazole ring were well tolerated and yielded potent PPAR $\gamma$  partial agonists. Among them, methoxy substitution at the 6-position of the benzisoxazole produced the most potent

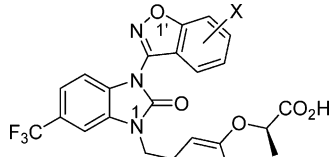
analogue (37) in PPAR $\gamma$  binding assay with an IC<sub>50</sub> of 4.1 nM. With 6-methoxybenzisoxazole as R<sub>2</sub> and the original acid moiety as R<sub>3</sub>, types and positions of R<sub>1</sub> were explored. Unlike the SAR in the indole series, both 6- and 5-substitutions on the benzimidazolone are equipotent, including the unsubstituted analogues. Trifluoromethyl and trifluoromethoxy groups remain the best substituents at either the 5- or 6-position (Table 3). With the rest of the structure optimized, the acidic moiety R<sub>3</sub> was extensively explored to maximize potency and optimize PK profiles, as well as to minimize off-target activity (Table 4). In the carboxylic acid series, meta-positioned phenoxy-(2*R*)-propanoic acid analogues with a *p*- or an *o*-chloro substitution (37, 42) continued to be the most potent PPAR $\gamma$  partial agonists. The direct analogue with a (*S*)-configuration (41) at the chiral center is about 10 times less active in binding and exhibits no activity in the functional assay. Analogues with no substitutions on the aryl (43) or larger substitutions on the  $\alpha$ -carbon (44) were significantly less active. The same SAR can be transferred to the corresponding analogues where the chiral phenoxy-carboxylic acid was replaced by a chiral oxazolidinone with the same configuration. Here again, the meta-substitution pattern was crucial for activity.

Table 1. SAR at N<sub>3</sub>-Substitution of the Benzimidazolone


Compound	R <sub>2</sub>	SPA-IC <sub>50</sub> (nM) <sup>a</sup> hPPAR <sub>γ</sub>	TA-EC <sub>50</sub> (nM) hPPAR <sub>γ</sub> (Max%) <sup>b</sup>
28		4800	3000 (17%)
29		255	489 (21%)
30		161	135 (15%)
31		1374	
32		68	200 (32%)

<sup>a</sup>SPA = scintillation proximity assay. Mean value of three determinations. <sup>b</sup>TA = transactivation assay. Rosiglitazone TA response set to 100%. Mean value of three determinations.

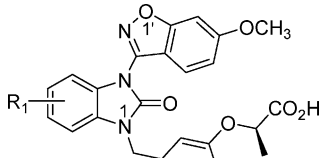
Table 2. SAR for Substitutions on the Benzisoxazole



Compound	X	SPA-IC <sub>50</sub> (nM) hPPAR <sub>γ</sub>	TA-EC <sub>50</sub> (nM) hPPAR <sub>γ</sub> (Max%)
33	7-CH <sub>3</sub>	9.2	4.1 (25%)
34	5-CH <sub>3</sub>	11.2	3000 (53%)
35	6-CH <sub>3</sub>	14.2	77.5 (37%)
36	5-Cl	35.4	120 (36%)
37	6-OCH <sub>3</sub>	4.1	103 (28)

Analogues with an ortho or a para substitution (**45** and **46**) were essentially inactive, while its meta-substituted counterpart (**47**) was a potent PPAR<sub>γ</sub> partial agonist. Removing the CH<sub>2</sub> linker between the benzimidazolone core and the phenyl group bearing the acid moiety resulted in a loss of activity (**48**). Similar to the carboxylic acid series, introducing chloro substitution on the aromatic ring bearing the acid moiety afforded the most potent analogue (**49**) with about 10-fold increase in potency.

Table 3. SAR for Substitutions on the Benzimidazolones

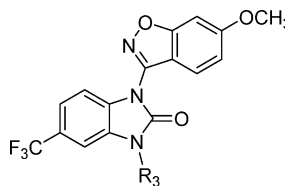


Compound	R <sub>1</sub>	SPA-IC <sub>50</sub> (nM) hPPAR <sub>γ</sub>	TA-EC <sub>50</sub> (nM) hPPAR <sub>γ</sub> (Max%)
37	6-CF <sub>3</sub>	4.1	103 (28%)
38	6-OCF <sub>3</sub>	3.2	11.4 (39%)
39	5-CF <sub>3</sub>	2.3	83 (43%)
40	5-OCF <sub>3</sub>	4.1	13.2 (31%)

It is important to note that all the compounds in this benzimidazolone series demonstrated a high degree of selectivity for PPAR<sub>γ</sub> vs the PPAR<sub>α</sub> and PPAR<sub>δ</sub> subtypes. No activity (>50 μM) was observed at these two receptors in binding assays. Mouse PPAR activities were measured for selected compounds and were found to be similar.

From the collection of potent SPPAR<sub>γ</sub>Ms synthesized in this series, the in vivo efficacy of selected analogues was evaluated using db/db mice by daily oral administration of the test compounds for 10 days.<sup>18</sup> On the 11th day, blood glucose (glu) levels from test animals were measured vs those from the vehicle control, with rosiglitazone at 10 mg/kg (10 mpk) as the positive control. Total exposures of test compounds in the animals were also measured at the end of the study. As shown in Table 5, despite being potent PPAR<sub>γ</sub> ligands in vitro with excellent pharmacokinetic profiles and moderate to high exposure levels, most of the analogues failed to generate robust glucose corrections in db/db mice except for compounds **51** and **52**. Many factors including plasma protein binding and tissue distribution could affect this outcome, and it has been difficult to fully evaluate these effects. Less protein binding may not transfer to increased efficacy for analogues with poor permeability. On the contrary, highly protein bound ligands could be more efficacious because of their preferential distribution to key tissues such as adipocytes. Since **51** and **52** are similar in structure to the rest of the analogues with comparable exposure levels and pharmacokinetic profiles, we speculate that their enhanced efficacies may be derived from their relatively higher activation levels in the transactivation assay. In repeated assays, the two compounds consistently produced PPAR<sub>γ</sub> activation of 70–101% relative to rosiglitazone while other benzimidazolone analogues were in the range of 18–50%. In the past, we have relied on reduced maximal agonism relative to that of rosiglitazone in the PPAR<sub>γ</sub> transactivation assay as a criterion for selecting partial agonists for in vivo evaluation. With activation levels almost as high as rosiglitazone, are compounds **51** and **52** still SPPAR<sub>γ</sub>Ms? To answer this question, a series of experiments were carried out to compare the activities of compound **51** and rosiglitazone head-to-head.

Compound **51** was cocrystallized with human PPAR<sub>γ</sub> ligand binding domain (LDB), and its structure was compared with those of rosiglitazone and pioglitazone, two prototypical thiazolidinedione-based PPAR<sub>γ</sub> full agonists. As shown in

Table 4. SAR of N<sub>1</sub>-Substitution at the Benzimidazolone


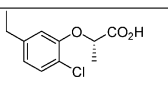
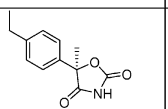
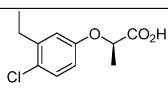
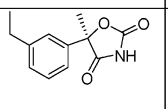
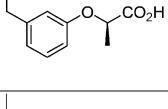
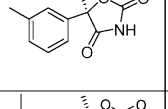
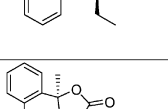
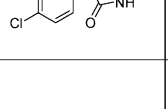
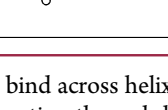
Cpd	R <sub>3</sub>	SPA	TA(Max%)	Cpd	R <sub>3</sub>	SPA	TA(Max%)
		hPPAR $\gamma$ (nM)				hPPAR $\gamma$ (nM)	
41		66	3000(4%)	46		2177	--
42		9.1	102 (26%)	47		93	237 (45%)
43		924	--	48		6935	--
44		3657	--	49		7.7	17 (28%)
45		6633	--				

Figure 1, the two full agonists bind across helix 3 with the acidic thiazolidinedione moiety interacting through hydrogen binding with Tyr-473 in helix 12, thereby stabilizing this activated receptor–ligand complex.<sup>19</sup> However, compound **51**, like other indole-based SPPAR $\gamma$ M reported earlier,<sup>20</sup> binds along the axis of helix 3 without interaction with Tyr-473 and helix 12. Its acidic oxazolidinedione moiety actually hydrogen-binds with Ser-342 far removed from Try-473 and helix 12. It is clear from the crystal structures that compound **51** binds to the human PPAR $\gamma$  receptor in a different mode than rosiglitazone. Its binding mode is actually very similar to that of other reported PPAR $\gamma$  partial agonists.<sup>21</sup>

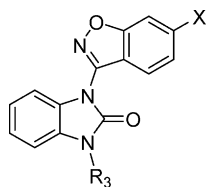
Tyr-473 is believed to play an important role in the stabilization of the LBD of the receptor by the full agonists. This amino acid residue lies within the helix 12 transcriptional activation function-2 domain that comprises a section of the transcriptional coactivator binding pocket of the LBD.<sup>22,23</sup> Many SPPAR $\gamma$ M lacking a direct interaction with Tyr-473 have been recently reported<sup>24–26</sup> to result in improved tolerability in preclinical animal testing. The apparent absence of an interaction between compound **51** and Tyr-473 based on the crystallographic data described above provides a physical basis for a differential biological response.

To further confirm the role that Tyr-473 plays in the binding between PPAR $\gamma$  full and partial agonists and the functional importance of this differential receptor–ligand interaction, recombinant mutagenesis techniques were employed to replace the Tyr-473 residue of PPAR $\gamma$  with an alanine.<sup>20</sup> The activities of compound **51** and rosiglitazone were then examined in transcriptional activity assays performed as described previously<sup>10</sup> in COS-1 cells transiently co-transfected with a GAL4-responsive reporter construct and a chimeric receptor

composed of the GAL4 DNA-binding domain and either the hPPAR $\gamma$ WT or hPPAR $\gamma$ Y473A LBD. As shown in Figure 2, rosiglitazone activity was dramatically reduced with hPPAR $\gamma$ Y473A relative to hPPAR $\gamma$ WT. In contrast, almost no changes in potency with compounds **51** and **52** were observed between the mutant and wild-type receptors. In our previous studies, many structurally diverse PPAR $\gamma$  full agonists and SPPAR $\gamma$ M were evaluated with hPPAR $\gamma$ WT and hPPAR $\gamma$ Y473A, and those data demonstrated that there were marked reductions in activation maxima for full agonists but not with SPPAR $\gamma$ M with the mutant receptor.<sup>20</sup> This result provides further physical evidence to support the assignment of compounds **51** and **52** as SPPAR $\gamma$ M.

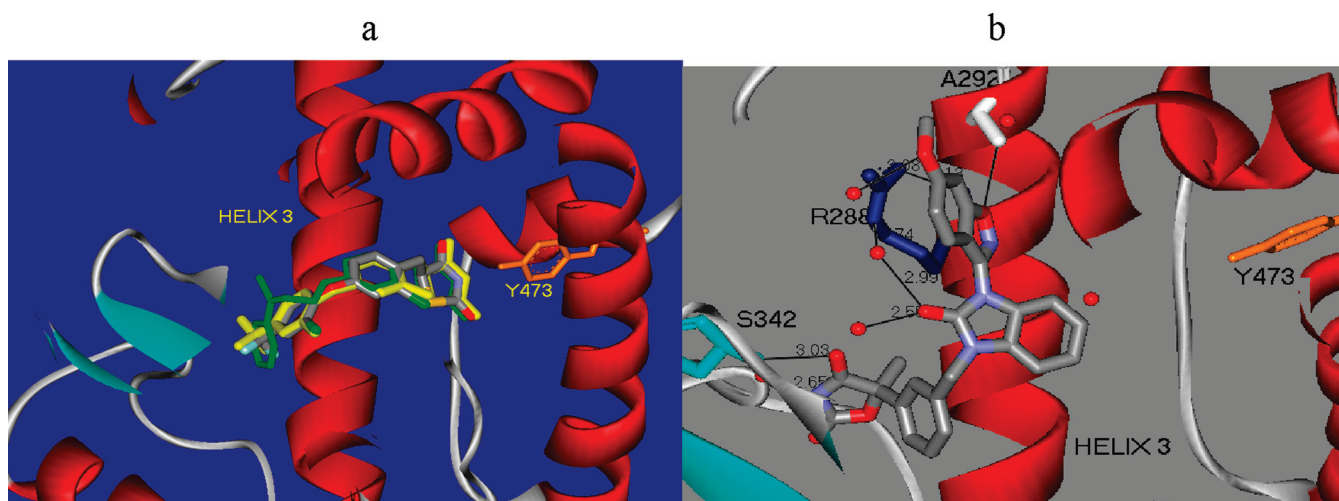
Ligand-dependent protein–protein interactions between nuclear receptors and their coactivators is a critical step in the regulation of transcription.<sup>27</sup> Agonist-induced conformational changes of the PPAR $\gamma$  LBD involves rearrangement of helices 3 and 12 that modulate the binding surface for various coactivators and co-repressors. Helices 3 and 12 are also directly involved in ligand binding.<sup>28</sup> Therefore, the binding of unique small molecule ligands to different amino acid residues of the PPAR $\gamma$  LBD could result in distinct conformational changes and PPAR $\gamma$ -co-activator affinities.<sup>29</sup> By use of a homogeneous time-resolved fluorescence (HTRF) assay,<sup>30</sup> PPAR $\gamma$ -co-activator affinity can be measured and quantified in terms of binding EC<sub>50</sub> and percent of activation. A panel of known nuclear receptor coactivators, including cAMP response element-binding protein (CBP),<sup>31</sup> peroxisome proliferator-activated receptor  $\gamma$  coactivator 1 (PGC-1),<sup>32</sup> steroid receptor coactivator 1 (Src-1),<sup>33</sup> and PPAR $\gamma$  binding protein (PBP),<sup>34</sup> were profiled in HTRF assays with a variety of PPAR $\gamma$  ligands. In these assays, compound **51** and other partial agonists were

Table 5. In Vitro and in Vivo Profiles of Selected Benzimidazolone Analogues



Compound	50	51	52	53	54
X	OCH <sub>3</sub>	OCH <sub>3</sub>	Cl	OCH <sub>3</sub>	OCH <sub>3</sub>
R <sub>3</sub>					
SPA -IC <sub>50</sub> hPPAR $\gamma$ (nM)	6.9	83.1	49.1	13.7	9.9
TA-EC <sub>50</sub> hPPAR $\gamma$ (nM) (Max%)	28.1 (31%)	360 (85%)	102 (101%)	51.1 (50%)	9.1 (26%)
Db -glu% <sup>a</sup>	30mpk 39%	10 mpk 74%	10 mpk 84%	30 mpk 30%	20 mpk 29%
Db exp. $\mu$ M <sup>b</sup>	576	159	1157	--	104
Rat PK <sup>c</sup>					
PO nAUC ( $\mu$ M.h)	1.5	4.3	1.9	5.0	0.8
Clp (mL/mm/kg)	11.4	5.5	26.5	7.3	29.7
T <sub>1/2</sub> (h)	5.0	4.2	3.0	6.9	3.8
F%	48	87	117	97	49

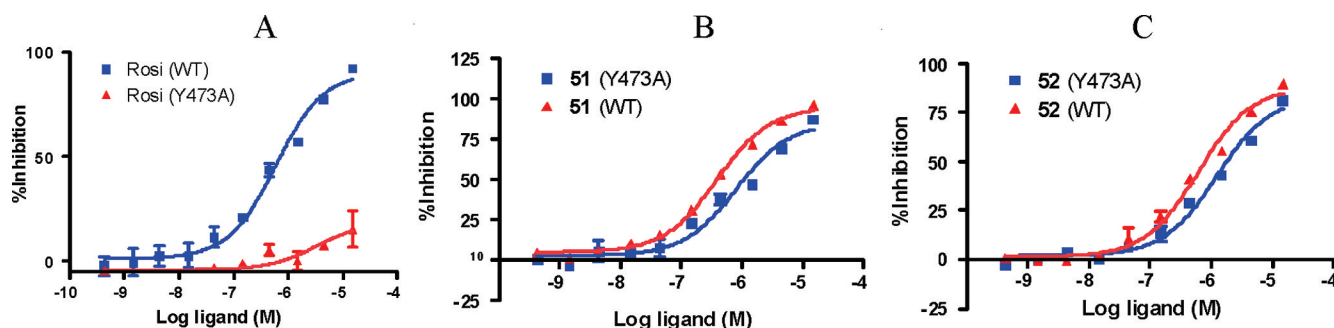
<sup>a</sup>Blood glucose levels of db/db mice orally administered with the test compounds were measured vs those from the vehicle control and expressed as % of corrections (glu%). <sup>b</sup>Total exposures of test compounds in the test animals were measured at the end of the study. <sup>c</sup>2 mpk po dosing in 5% methylcellulose; 0.5 mpk iv dosing in ethanol/PEG400/water (1/4/5).



**Figure 1.** PPAR $\gamma$  ligand binding domain showing ligand–protein interactions of (a) full PPAR $\gamma$  agonists rosiglitazone (green) and pioglitazone (yellow) (PDB access code 2PRG) and (b) PPAR $\gamma$  selective modulator, compound 51 (gray) (PDB access code 3TY0). The helix 3 region is marked, and the tyrosine 473 residue is shown in orange.

compared with PPAR $\gamma$  full agonists including rosiglitazone. As shown in Table 6, the full agonists displayed potent binding affinities and a high level of activation on all four coactivators. The SPPAR $\gamma$ M<sub>s</sub>, however, showed diverse binding potencies

and activation levels toward these different coactivators, and all SPPAR $\gamma$ M<sub>s</sub> produced attenuated levels of activation compared to full agonists. In general, SPPAR $\gamma$ M<sub>s</sub> tended to have a relatively higher level of activation on PGC-1 and PBP but



**Figure 2.** SPA binding potencies of PPAR $\gamma$  ligands with hPPAR $\gamma$ Y473A versus hPPAR $\gamma$ WT: (A) binding of rosiglitazone to hPPAR $\gamma$ Y473A and hPPAR $\gamma$ WT; (B) binding of **51** to hPPAR $\gamma$ Y473A and hPPAR $\gamma$ WT; (C) binding of **52** to hPPAR $\gamma$ Y473A and hPPAR $\gamma$ WT.

**Table 6.** Coactivator Recruiting Patterns between Full and Partial Agonists<sup>a</sup>

compd	CBP1-453		PGC1		Src1		PBP	
	EC <sub>50</sub> ( $\mu$ M)	Max (%)	EC <sub>50</sub> ( $\mu$ M)	Max (%)	EC <sub>50</sub> ( $\mu$ M)	Max (%)	EC <sub>50</sub> ( $\mu$ M)	Max (%)
rosiglitazone	0.046	105	0.11	82	0.2	84	0.03	104
farglitazar <sup>37</sup>	0.005	112	0.004	124	0.006	167	0.003	100
SB219994 <sup>38</sup>	0.001	101	0.001	77	0.002	90	0.001	107
<b>1a</b>	0.006	50	0.005	52	>50	16	0.005	74
<b>1b</b>	0.007	54	0.005	67	0.009	18	0.006	89
<b>30</b>	0.48	31	0.46	48	>50	0	0.44	54
<b>32</b>	>50	9	3.24	63	>50	0	>50	8
<b>50</b>	>50	15	0.002	44	>50	0	0.003	40
<b>51</b>	0.06	67	0.029	71	0.13	23	0.01	96
<b>53</b>	0.011	14	0.008	19	>50	0	0.011	21
<b>54</b>	>50	10	0.002	29	>50	0	1.82	55

<sup>a</sup>Homogeneous time-resolved fluorescence (HTRF) assay of PPAR ligands with cAMP response element-binding protein (CBP), peroxisome proliferator-activated receptor  $\gamma$  coactivator 1 (PGC-1), steroid receptor coactivator 1 (Src-1), and PPAR $\gamma$  binding protein (PBP). Full titrations were conducted for all compounds from 15  $\mu$ M down with WT hPPAR LBD. The PPAR $\gamma$  full agonist, 3-chloro-4-(3-(3-phenyl-7-propylbenzofuran-6-yloxy)propylthio)phenylacetic acid (L-796449)<sup>39</sup> was used as the 100% response control for each of the four coactivators. Rosiglitazone, farglitazar, and 4-[2-(2-benzoxazolylmethylamino)ethoxy]- $\alpha$ -(2,2,2-trifluoroethoxy)-( $\alpha$ S)-benzenepropanoic acid (SB219994) were used as full agonist control.

moderate to no activation on CBP-1 and Src-1. The coactivator recruiting pattern of compound **51** was in general agreement with the other partial agonists. It recruited PGC-1 with a 71% efficiency compared with 83% of rosiglitazone at a final concentration of 15  $\mu$ M but was only 23% efficient in binding to Src-1 relative to rosiglitazone's 84%. It is worth noting that the activation level of compound **51** on PGC-1 was among the highest in partial agonists tested, and it was also one of the most efficacious partial agonists in db/db mice study for glucose correction. This result is consistent with findings in several recent publications that PGC-1 is preferably recruited by SPPAR $\gamma$ Ms vs other coactivators and has been shown to be more directly associated with insulin sensitization efficacy.<sup>35</sup> This coactivator was also found to be critical in preventing triglyceride accumulation and potentiating insulin signaling.<sup>36</sup>

Compound **51** was also evaluated in microarray gene expression studies using differentiated 3T3-L1 adipocytes. A collection of PPAR $\gamma$  full and partial agonists were tested for effects on expression levels of 4619 reporter genes believed to be directly or indirectly regulated by PPAR $\gamma$  activation.<sup>40</sup> The gene signature of **51** was similar to those of other SPPAR $\gamma$ Ms, demonstrating a  $\gamma$  activation index (GAI)<sup>12d</sup> of 0.71 relative to 1.0 for rosiglitazone and most other full agonists.

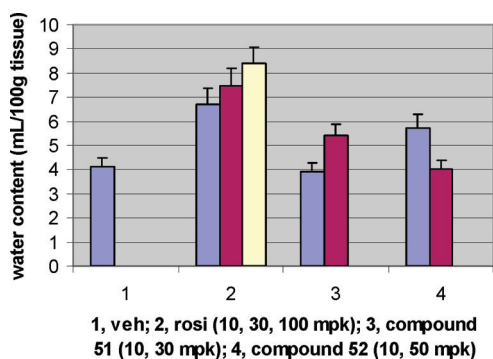
Multidosing studies of **51** in db/db mice were carried out with simultaneous monitoring of blood glucose and drug exposure levels. As shown in Table 7, compound **51** produced dose- and exposure-dependent glucose corrections in this diabetic mouse model with efficacy equivalent to or slightly

**Table 7.** Multidosing db/db Studies of Compound **51**<sup>a</sup>

parameter	compd <b>51</b>					rosiglitazone
	3	10	20	25	30	
dose (mpk)	3	10	20	25	30	10
glucose (%) <sup>b</sup>	49	74	77	84	87	60–80
AUC ( $\mu$ M·h) <sup>b</sup>	70	129			450	220–720 <sup>c</sup>

<sup>a</sup>Male db/db mice and lean mice were dosed daily for 11 days by gavage with vehicle or the indicated doses of test compounds. Glucose corrections were calculated as percent correction of vehicle control. <sup>b</sup>Mean value ( $n = 7$ ).  $P < 0.01$  vs vehicle control. <sup>c</sup>Mean value ( $n = 4$ ).

better than rosiglitazone. At 10 mpk and an exposure of 129  $\mu$ M, compound **51** produced a glucose correction of 74% compared to the 60–80% glucose lowering by 10 mpk rosiglitazone with exposures ranging from 220 to 720  $\mu$ M (based on historical data). At 20, 25, and 30 mpk, compound **51** continued to show improved glucose correction of 77%, 84%, and 87%, respectively. In a parallel experiment, the water content of the epididymal fat pad (EWAT) of the db/db mice treated with compounds **51** and **52** and rosiglitazone were measured vs that of the untreated group. In contrast to rosiglitazone which caused significant dose dependent water content increase in EWAT at 10, 30, and 100 mpk, compounds **51** and **52** generated almost no change of water content at the equally efficacious doses of 10 and 30 mpk, and 10 and 50 mpk, respectively (Figure 3). These results suggest a diminished propensity of these SPPAR $\gamma$ Ms to induce edema in comparison



**Figure 3.** PPAR $\gamma$  full agonist rosiglitazone vs SPPAR $\gamma$ M 51 and 52 in EWAT water content in db/db mice. Male db/db mice were dosed as described in the in vivo db/db mouse studies. At the end of day 11 dosing, epididymal fat pad tissue (EWAT) of test animal was obtained and water content was determined by vacuum drying. Data are displayed as mean value of seven determinations.

with PPAR $\gamma$  full agonists at comparable levels of antihyperglycemic efficacy.

To further evaluate compound 51 in vivo as a SPPAR $\gamma$ M, a 7-day study was conducted in obese, insulin resistant Zucker fa/fa rats,<sup>40</sup> a preclinical model we used to directly compare the insulin sensitizing efficacy vs the mechanism-based side effects of PPAR $\gamma$  ligands. The plasma volume (PV) and heart weight of test animals were measured as well as their insulin levels and lipid profiles. At the conclusion of the study, compound 51 (0.1, 1.0, 10, 100 mpk) was compared to rosiglitazone (1.0, 10, and 100 mpk). Both compounds substantially lowered elevated levels of free fatty acids, insulin, and triglycerides, indicating significant insulin sensitizing activity. However, efficacy was achieved with a slightly lower exposure of compound 51 (insulin lowering ED<sub>50</sub> = 281  $\mu$ M·h) than rosiglitazone (insulin lowering ED<sub>50</sub> = 312  $\mu$ M·h). Importantly, while rosiglitazone produced clear dose responsive increases in plasma volume and heart weight at dosages of  $\geq$ 10 mpk, no significant increase in heart weight was seen with compound 51. Although a modest increase in plasma volume was observed with compound 51 at the highest dose tested, it was much diminished in comparison with rosiglitazone, especially at the higher doses (Figure 4).

Another attractive feature of the benzimidazolones was revealed in counterscreening assays. For instance, in a screen of cytochrome P450 isozymes for potential inhibition, 51 showed

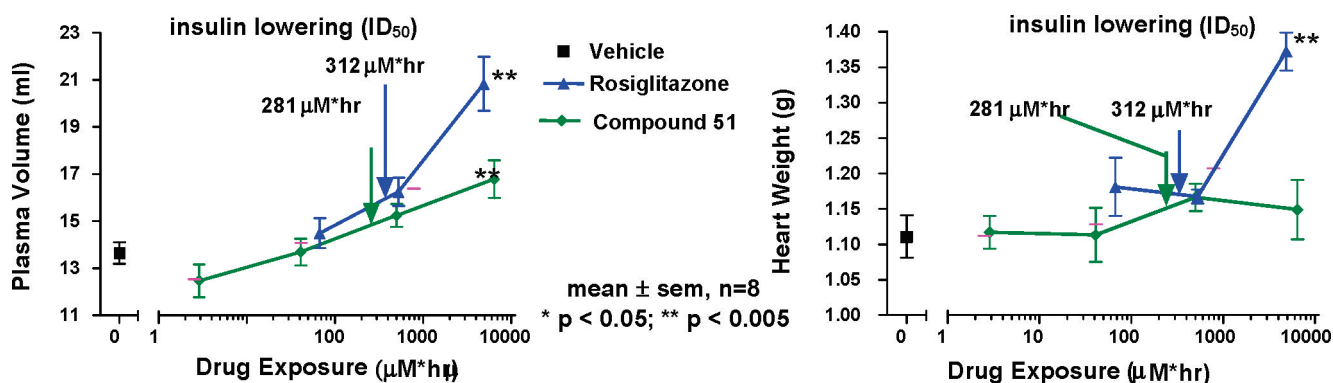
IC<sub>50</sub> values of 91, 22, 10, and 2  $\mu$ M, respectively, for 2D6, 3A4, 2C8, and 2C9, an improved profile over some of the indole analogues. In addition, a receptor panel screen (140 assays, Panlabs) of 51 revealed only one assay (serine/threonine kinase, 0.951  $\mu$ M) with activity under 1  $\mu$ M and no ion channel (IKr and PXR) activities at concentrations of up to 10  $\mu$ M.

## CONCLUSION

A new class of potent and highly selective PPAR $\gamma$  partial agonists based on the benzimidazolone platform was discovered by rational design. Large numbers of analogues were prepared through a convergent synthetic strategy, and their SARs were extensively explored. Replacement of the indole core with benzimidazolone resulted in a significant increase in PPAR $\gamma$  selectivity over PPAR $\alpha$  and PPAR $\delta$  with moderate improvements in off-target activities. Substituted benzisoxazoles are preferred over other aryl, alkyl, and acyl groups as R<sub>2</sub> for occupying the hydrophobic region of the receptor. Use of chiral oxazolidinones in place of phenoxyacetic acids as the acidic moiety (R<sub>3</sub>) generally enhances pharmacokinetic profiles. The lead compound, 51, displayed robust glucose and insulin lowering activity similar or superior to that of rosiglitazone in rodent models of T2DM. Unlike thiazolidinediones and other carboxylic acid based PPAR $\gamma$  full agonists, this new class of compounds behaves as selective PPAR $\gamma$  modulators (SPPAR $\gamma$ M). This designation is supported by X-ray crystallographic analysis and mutagenesis studies as well as their unique profiles in recruiting a panel of nuclear receptor coactivators. Preferential recruitment of PGC-1 and PBP over other coactivators by 51 may contribute to its enhanced in vivo efficacy compared to other similar partial agonists in its class. Plasma volume expansion and cardiac hypertrophy were diminished with 51 vs that caused by rosiglitazone in obese, insulin resistant fa/fa rats. These unique biological properties displayed by SPPAR $\gamma$ M 51 make it an attractive candidate for further evaluation as a potential therapeutic agent in the treatment of T2DM.

## EXPERIMENTAL SECTION

**In Vitro Assays.** Activities of compounds were evaluated for both binding affinity and functional activity. Binding affinities for the PPARs were measured in a scintillation proximity assay (SPA) as previously described.<sup>10a</sup> Selected compounds from the binding assay were then evaluated for their potencies of PPAR gene activation in cell-based



**Figure 4.** Evaluation of 51 in fa/fa Zucker rat for plasma volume and cardiac effects. Animals ( $n = 8$ ) were treated daily for 7 days with vehicle, rosiglitazone (1, 10, and 100 mpk), or 51 (0.1, 1.0, 10, 100 mpk). Circulating drug and insulin levels, plasma volume, and heart weight were determined as described in the Experimental Section. The drug exposure levels associated with a 50% reduction in plasma insulin (ED<sub>50</sub>) for rosiglitazone and 51 were 312 and 281  $\mu$ M·h, respectively.



transcription assays (TA) using GAL4-PPAR chimeric receptors as previously described.<sup>20</sup> Homogeneous time-resolved fluorescence (HTRF) assays of PPAR ligands with selected nuclear receptor coactivators were carried out according to literature methods.<sup>40</sup> All results were produced in triplicate, and mean values are reported.

**In Vivo db/db Mouse Studies.** Male db/db (C57BLKS/J-m +/-Leprdb) mice at 12–13 weeks of age and nondiabetic db/+ (lean) mice from Jackson Laboratories were housed seven mice per cage and fed a rodent chow with free access to water. Mice (seven per group) received a once daily dose of test compounds with vehicle (0.25% methylcellulose) by oral gavage for 11 days. Blood was collected from the tail immediately prior to the next dosing at days 0, 4, 7, and 11 for measurement of the plasma glucose levels.

**Evaluation of Insulin Sensitization.** Tail nick blood samples were collected 1 day before the start of dosing and 1 day after the seventh dose. Plasma glucose (Sigma glucose Trinder assay kit, St. Louis, MO, U.S.), insulin (rat insulin RIA from American Laboratory Products Company, Windham, NH, U.S.), free fatty acids (FFA), and triglyceride (both from Roche Diagnostics, Basel, Switzerland) concentrations were determined following the methods provided by the manufacturers.

**Tissue Water Content Measurements.** Immediately after euthanasia, epididymal fat pads were removed and weighed and placed in individual glass scintillation vials. Weighed tissues were subjected to a vacuum-applied Speed Vac centrifugation/drying process over a 24 h period. After this drying process, tissues were weighed again to calculate individual tissue water content.

**Plasma Volume Measurement.** After determination of extracellular fluid volume, plasma volume was measured in anesthetized animals using a dye dilution technique following methods described by Belcher and Harriss<sup>38</sup> with minor modifications. Evans blue dye solution (25 mg/mL in physiological saline) was filtered through a 0.22  $\mu$ m filter prior to injection into a femoral vein. Twenty minutes after injection, a heparinized blood sample (2 mL) was withdrawn from the descending aorta. Plasma was separated by centrifugation of the blood at 1100g for 15 min; samples were kept at  $-80^{\circ}\text{C}$  until assayed. Absorbance of the thawed plasma was read at 620 nm, and plasma Evans blue dye concentrations were calculated according to a standard curve generated by a serial dilution of the 25 mg/mL Evans blue dye saline solution. Plasma volume was calculated by using the dilution factors of Evans blue as shown below.

$$\text{plasma volume} = \frac{[\text{dye}] \text{ injected} \times \text{volume of dye injected}}{[\text{dye}] \text{ in plasma}}$$

**Heart Weight Measurements.** Animals were then euthanized by pneumothorax and exsanguination, and the heart was excised, blotted, and weighed.

**Pharmacokinetic Studies.** For the determination of test compound exposures in animals, blood samples were taken at specified intervals. The plasma was separated, acidified by the addition of 0.5 M formate buffer, pH 3.0 (0.3 mL of formate buffer per mL plasma), and stored at  $-70^{\circ}\text{C}$  prior to extraction and analysis. Concentrations of the test compounds were determined following protein precipitation with acetonitrile. Calibration curves were constructed using plasma of control animals by addition of known quantities of the testing compounds as an internal standard. Quantitative analysis was carried out by LC–MS–MS using a PE Sciex API 3000 triple quadrupole mass spectrometer. Plasma concentrations and PK parameters were determined using Watson software.

**X-ray Crystallography Studies.** Purified PPAR $\gamma$  LBD (residues Gln-203 to Tyr-477) was mixed with compound **51** at 1.1:1 M ratio of compound/protein on ice and allowed to stand at  $4^{\circ}\text{C}$  overnight. Crystals were grown by vapor diffusion at room temperature in a Cryschem MVD-24 crystallization tray (Charles Supper, Natick, MA). A suitable crystal was selected, and its X-ray diffraction data were collected at the ID-17 beamline of the Industrial Macromolecular Crystallography Association Collaborative Access Team. The structure

of compound **51** was resolved to 2.35 Å. The refined coordinates have been deposited at the Protein Data Bank with access code of 3TY0.

**Synthetic Materials and Methods.** Reagents and solvents were obtained from commercial suppliers and were used without further purification. Flash chromatography was performed using E. Merck silica gel (230–400 mesh).  $^1\text{H}$  NMR spectra were recorded in the deuterated solvents specified on a Varian Unity INOVA 500 MHz instrument. Chemical shifts are reported in ppm in the indicated solvent with TMS as internal standard. LC–MS was conducted using HP1100 and Micromass ZQ instruments. Elemental analysis results were obtained from Robertson Microlit Laboratories. Purities of all compounds reported were above 95% determined by high performance liquid chromatography (HPLC) with UV detection at two wavelengths of 220 and 254 nm. Purities of key compounds were also confirmed by elemental analyses.

**1-Boc-5-Trifluoromethylbenzimidazole-2-one and 1-Boc-6-Trifluoromethylbenzimidazole-2-one (7a, R<sub>1</sub> = 5-CF<sub>3</sub>; 7b, R<sub>1</sub> = 6-CF<sub>3</sub>).** To a solution of 5-trifluoromethylbenzimidazole-2-one (25 g, 123 mmol) in DMF (150 mL) was added NaH (95%, 3.5 g, 148 mmol). The reaction mixture was stirred at room temperature for 2 h followed by addition of di-*tert*-butyl dicarbonate (27 g, 123 mmol). The mixture was stirred at room temperature overnight, diluted with water (400 mL), and extracted with ethyl acetate (2  $\times$  150 mL). The organic extract was washed with water (2  $\times$  100 mL) and brine (100 mL), dried over anhydrous MgSO<sub>4</sub>, and concentrated under vacuum. The residue was chromatographed on silica gel with hexane/ethyl acetate (3:1) as the solvent system to obtain 9.2 g (25% yield) of 1-Boc-5-trifluoromethylbenzimidazole-2-one (**7a**) as an earlier eluted product.  $^1\text{H}$  NMR (CDCl<sub>3</sub>, 500 MHz)  $\delta$  9.79 (brs, 1H), 7.87 (d, 1H), 7.45 (d, 1H), 7.43 (s, 1H), 1.72 (s, 9H). LC–MS (ESI): >95% purity at  $\lambda$  220 and 254 nm. MS:  $m/z$  303.09 [M + H]<sup>+</sup>. Fractions containing the later eluted product were combined and concentrated to dryness to obtain 17.5 g (47% yield) of 1-Boc-6-trifluoromethylbenzimidazole-2-one (**7b**).  $^1\text{H}$  NMR (CDCl<sub>3</sub>, 500 MHz)  $\delta$  9.98 (brs, 1H), 8.09 (s, 1H), 7.49 (d, 1H), 7.23 (d, 1H), 1.76 (s, 9H). LC–MS (ESI): >95% purity at  $\lambda$  220 and 254 nm. MS:  $m/z$  303.09 [M + H]<sup>+</sup>.

**1-(4-Chlorobenzyl)-5-trifluoromethylbenzimidazole-2-one (9a, R<sub>1</sub> = 5-CF<sub>3</sub>, R<sub>2</sub> = 4-Chlorobenzyl).** To the solution of 1-Boc-6-trifluoromethylbenzimidazole-2-one (**7b**, 100 mg, 0.33 mmol) in DMF (2 mL) were added 4-chlorobenzyl bromide (81 mg, 0.39 mmol) and Cs<sub>2</sub>CO<sub>3</sub> (300 mg, 0.92 mmol). The mixture was stirred at room temperature for 2 h, diluted with water (4 mL), and extracted with ethyl acetate (2  $\times$  3 mL). The organic extracts were combined and concentrated to obtain a solid. The solid was dissolved in TFA (1.5 mL). The mixture was stirred at room temperature for 2 h, and concentrated to dryness. The residue was purified by silica gel chromatography with hexane/ethyl acetate (4:1) as solvent system to obtain 90 mg (84% yield) of a white solid.  $^1\text{H}$  NMR (DMSO-*d*<sub>6</sub>, 500 MHz)  $\delta$  9.35 (brs, 1H), 7.38 (s, 1H), 7.34 (d, 2H), 7.28 (d, 2H), 7.27 (d, 1H), 6.93 (d, 1H), 5.10 (s, 2H). LC–MS (ESI): >95% purity at  $\lambda$  220 and 254 nm. MS:  $m/z$  327.0 [M + H]<sup>+</sup>.

**1-(4-Chlorobenzyl)-5-trifluoromethylbenzimidazole-2-one (9b, R<sub>1</sub> = 5-CF<sub>3</sub>, R<sub>2</sub> = 4-Chlorobenzyl).** To the solution of 1-Boc-6-trifluoromethylbenzimidazole-2-one (**7b**, 200 mg, 0.66 mmol) in anhydrous pyridine (4 mL) was added 4-chlorobenzoyl chloride (115 mg, 0.66 mmol). The mixture was stirred at room temperature overnight and concentrated to dryness. The residue was dissolved in TFA (2 mL) and stirred at room temperature for 2 h. The mixture was concentrated to dryness and purified by silica gel column chromatography to obtain 200 mg (90% yield) of a solid.  $^1\text{H}$  NMR (DMSO-*d*<sub>6</sub>, 500 MHz)  $\delta$  7.92 (d, 1H), 7.81 (d, 2H), 7.56 (d, 2H), 7.66 (brs, 1H), 7.48 (d, 1H), 7.32 (brs, 1H). LC–MS (ESI): >95% purity at  $\lambda$  220 and 254 nm. MS:  $m/z$  341.0 [M + H]<sup>+</sup>.

**1-(4-*tert*-Butylphenyl)-5-trifluoromethylbenzimidazole-2-one (9c, R<sub>1</sub> = 5-CF<sub>3</sub>, R<sub>2</sub> = 4-*tert*-Butylphenyl).** To the solution of 1-Boc-6-trifluoromethylbenzimidazole-2-one (**7b**, 870 mg, 2.88 mmol) in methylene chloride (100 mL) were added 4-*tert*-butylphenylboronic acid (960 mg, 2.88 mmol), Cu(OAc)<sub>2</sub> (521 mg, 2.88 mmol), triethylamine (0.94 mL, 14 mmol), and molecular sieves (4 Å, 200 mg). The mixture was stirred at room temperature under open air

overnight and filtered. The filtrate was concentrated to dryness. The residue was dissolved in TFA (5 mL), stirred at room temperature for 3 h, and concentrated to dryness. The residue was redissolved in ethyl acetate (5 mL) and passed through a silica gel column and washed with hexane/ethyl acetate (3:1) (500 mL). The filtrate was concentrated to obtain 800 mg (84 yield) of a solid. LC–MS (ESI): >95% purity at  $\lambda$  220 and 254 nm. MS:  $m/z$  334.0 [M + H]<sup>+</sup>.

**1-[(6-Chloro)benzisoxazol-3-yl]-5-trifluoromethylbenzimidazole-2-one (9d, R<sub>1</sub> = 5-CF<sub>3</sub>, R<sub>2</sub> = 6-Chlorobenzisoxazol-3-yl) and 1-[(6-Chloro)benzisoxazol-3-yl]-6-trifluoromethylbenzimidazole-2-one (9e, R<sub>1</sub> = 6-CF<sub>3</sub>, R<sub>2</sub> = 6-Chlorobenzisoxazol-3-yl).**

To a solution of 1-Boc-6-trifluoromethylbenzimidazole-2-one (7b, 800 mg, 264 mmol) in DMF (4 mL) was added 3,6-dichlorobenzisoxazole (500 mg, 264 mmol) and Cs<sub>2</sub>CO<sub>3</sub> (1.5 g, 570 mmol). The suspension was heated to 150 °C in an oil bath and stirred overnight. The mixture was then cooled to room temperature, diluted with water (5 mL), and extracted with ethyl acetate (3 × 5 mL). The organic extracts were combined, dried over anhydrous MgSO<sub>4</sub>, and concentrated to dryness. The residue was purified by silica gel column chromatography using hexane/ethyl acetate (4:1) as solvent system. Fractions containing earlier eluted product were combined and concentrated to obtain 140 mg (15% yield) of 1-[3-(6-chloro)benzisoxazol-3-yl]-5-trifluoromethylbenzimidazole-2-one (9d) as a white solid. <sup>1</sup>H NMR (CDCl<sub>3</sub>, 500 MHz)  $\delta$  8.72 (brs, 1H), 8.29 (s, 1H), 7.96 (d, 1H), 7.64 (m, 2H), 7.52 (d, 1H), 7.44 (s, 1H). LC–MS (ESI): >95% purity at  $\lambda$  220 and 254 nm. MS:  $m/z$  370.1 [M + H]<sup>+</sup>.

Fractions containing later eluted product were combined and concentrated to obtain 46 mg (5% yield) of 1-[3-(6-chloro)benzisoxazol-3-yl]-6-trifluoromethylbenzimidazole-2-one (9e) as a white solid. <sup>1</sup>H NMR (CDCl<sub>3</sub>, 500 MHz)  $\delta$  8.44 (brs, 1H), 8.30 (s, 1H), 8.18 (s, 1H), 7.64 (m, 2H), 7.55 (d, 1H), 7.25 (d, 1H). LC–MS (ESI): >95% purity at  $\lambda$  220 and 254 nm. MS:  $m/z$  370.1 [M + H]<sup>+</sup>.

**1-[(6-Chloro)benzisoxazol-3-yl]-5-trifluoromethoxybenzimidazole-2-one (9f, R<sub>1</sub> = 5-OCF<sub>3</sub>, R<sub>2</sub> = 6-Chlorobenzisoxazol-3-yl) and 1-[(6-Chloro)benzisoxazol-3-yl]-6-trifluoromethoxybenzimidazole-2-one (9g, R<sub>1</sub> = 6-OCF<sub>3</sub>, R<sub>2</sub> = 6-Chlorobenzisoxazol-3-yl).** To a solution of 1-Boc-6-trifluoromethoxybenzimidazole-2-one (7d, R<sub>1</sub> = 6-OCF<sub>3</sub>, 5 g, 15.7 mmol) in DMF (20 mL) were added 3,6-dichlorobenzisoxazole (3.0 g, 15.7 mmol) and Cs<sub>2</sub>CO<sub>3</sub> (11 g, 31.4 mmol). The suspension was heated to 150 °C in an oil bath and stirred overnight. The mixture was then cooled to room temperature, diluted with water (30 mL), and extracted with ethyl acetate (2 × 20 mL). The organic extracts were combined, dried over anhydrous MgSO<sub>4</sub>, and concentrated to dryness. The residue was purified by silica gel column chromatography using hexane/ethyl acetate (4:1) as solvent system. Fractions containing earlier eluted product were combined and concentrated to obtain 2.4 g (40% yield) of 1-[3-(6-chloro)benzisoxazol-3-yl]-5-trifluoromethoxybenzimidazole-2-one (9f) as a white solid. <sup>1</sup>H NMR (DMSO-*d*<sub>6</sub>, 500 MHz)  $\delta$  8.28 (d, 1H), 8.12 (s, 1H), 7.74 (s, 1H), 7.54 (d, 1H), 7.14 (m, 2H). LC–MS (ESI): >95% purity at  $\lambda$  220 and 254 nm. MS:  $m/z$  370.1 [M + H]<sup>+</sup>. Fractions containing later eluted product were combined and concentrated to obtain 1.3 g (19.1% yield) of 1-[3-(6-chloro)benzisoxazol-3-yl]-6-trifluoromethoxybenzimidazole-2-one (9g) as a white solid. <sup>1</sup>H NMR (DMSO-*d*<sub>6</sub>, 500 MHz)  $\delta$  8.28 (d, 1H), 8.12 (s, 1H), 7.66 (s, 1H), 7.54 (d, 1H), 7.22 (m, 2H). LC–MS (ESI): >95% purity at  $\lambda$  220 and 254 nm. MS:  $m/z$  370.1 [M + H]<sup>+</sup>.

**1-[(6-Methoxy)benzisoxazol-3-yl]-6-trifluoromethoxybenzimidazole-2-one (9h, R<sub>1</sub> = 6-OCF<sub>3</sub>, R<sub>2</sub> = 6-Methoxybenzisoxazol-3-yl).** To a solution of 1-[3-(6-chloro)benzisoxazol-3-yl]-6-trifluoromethoxybenzimidazole-2-one (9g, 1.2 g, 3.25 mmol) in DMF (5 mL) was added NaOMe solution in methanol (30 wt %/wt, 20 mL). The mixture was heated to 80 °C under vacuum to remove residual methanol and then stirred at 110 °C under nitrogen overnight. The mixture was then cooled to room temperature, diluted with water (50 mL), and adjusted to pH 6 with 10% aqueous HCl. The resulting suspension was stirred in an ice bath for 2 h and filtered. The solid was washed with water and dried in an oven (90 °C) for 2 h and then under high vacuum at room temperature for 3 h to obtain 1.1 g (93% yield) of a slightly yellow solid. LC–MS (ESI): >95% purity at  $\lambda$  220 and 254 nm. MS:  $m/z$  366.0 [M + H]<sup>+</sup>.

**1-(6-Chlorobenzisoxazol-3-yl)benzimidazole-2-one (9i, R<sub>1</sub> = H, R<sub>2</sub> = 6-Chlorobenzisoxazol-3-yl) and 1-(6-Methoxybenzisoxazol-3-yl)benzimidazole-2-one (9j, R<sub>1</sub> = H, R<sub>2</sub> = 6-Methoxybenzisoxazol-3-yl).** To a solution of benzimidazole-2-one (Aldrich, 1.1 g, 7.5 mmol) in DMF (20 mL) was added 3,6-dichlorobenzisoxazole (1.5 g, 7.5 mmol) and Cs<sub>2</sub>CO<sub>3</sub> (4.8 g, 15 mmol). The suspension was heated to 150 °C in an oil bath and stirred overnight. The mixture was then cooled to room temperature, diluted with water (30 mL), and stirred in an ice bath for 2 h. The mixture was then filtered. The solid was washed with water and dried under high vacuum to obtain 2.0 g (93% yield) of a yellow solid as 1-(6-chlorobenzisoxazol-3-yl)benzimidazole-2-one (9i). LC–MS (ESI): >95% purity at  $\lambda$  220 and 254 nm. MS:  $m/z$  286.1 [M + H]<sup>+</sup>.

To the solution of the above product (1.0 g, 3.5 mmol) in DMF (15 mL) was added NaOMe solution in methanol (30 wt %/wt, 10 mL). The mixture was heated to 80 °C under vacuum to remove residual methanol and then stirred at 110 °C under nitrogen overnight. The mixture was then cooled to room temperature, diluted with water (50 mL), and adjusted to pH 6 with 10% aqueous HCl. The resulting suspension was stirred in an ice bath for 2 h and filtered. The solid was washed with water and dried in an oven (90 °C) for 2 h and then under high vacuum at room temperature for 3 h to obtain 1.1 g (93% yield) of a slightly yellow solid (9j). LC–MS (ESI): >95% purity at  $\lambda$  220 and 254 nm. MS:  $m/z$  282.10 [M + H]<sup>+</sup>.

**2-(3-Methylphenyl)propene (21a, Y = H).** To a suspension of methyltriphenylphosphonium bromide (33.2 g, 92.9 mmol) in diethyl ether (200 mL) at room temperature was added slowly *n*-BuLi (2.5 M in hexanes, 37 mL). The resulting yellow solution was stirred for 30 min before 3-methylacetophenone (12 mL, 90 mmol) was introduced. The mixture was stirred at room temperature overnight. The precipitate was removed by filtration. The solvent was removed in vacuum. Purification by flash chromatography gave 8 g (67% yield) of the 2-(3-methylphenyl)propene product.

**(2R)-(3-Methylphenyl)-1,2-propane-diol (22a, Y = H).** To a suspension of AD-mix- $\beta$  (7 g) in H<sub>2</sub>O/*t*BuOH (25 mL/25 mL) at 0 °C was added 2-(3-methylphenyl)propene (21a) (0.66 g, 5 mmol). The reaction mixture was stirred at 0 °C overnight. Na<sub>2</sub>SO<sub>3</sub> (7.5 g) was added. After 1 h at room temperature, the mixture was extracted with EtOAc (3×). The combined organic layers were washed with brine, dried over MgSO<sub>4</sub>, filtered, and concentrated in vacuum. Purification by flash chromatography gave 0.71 g (82% yield) of (2R)-(3-methylphenyl)-1,2-propane-diol. LC–MS (ESI): >95% purity at  $\lambda$  220 and 254 nm. MS:  $m/z$  167.1 [M + H]<sup>+</sup>.

**(2R)-2-Hydroxy-2,3-dimethylbenzeneacetic Acid (23a, Y = H).** To a solution of (2R)-(3-methylphenyl)-1,2-propane-diol (22a) (0.7 g, 4.2 mmol) in water (50 mL) were added NaHCO<sub>3</sub> (0.4 g, 5.5 mmol) and 10% Pt/C (0.7 g). Air was bubbled through the reaction mixture via a gas dispenser at 70 °C overnight. The mixture was cooled to room temperature and filtered through Celite. The filtrate was acidified with aqueous H<sub>2</sub>SO<sub>4</sub> (1.0 N) to pH 2 and extracted with EtOAc (3×). The combined organic layers were washed with brine, dried over MgSO<sub>4</sub>, filtered, and concentrated in vacuum to give 0.66 g (88% yield) of the acid. <sup>1</sup>H NMR (DMSO-*d*<sub>6</sub>, 500 MHz)  $\delta$ : 7.32 (s, 1H), 7.28 (d, 1H), 7.19 (t, 1H), 7.02 (d, 1H), 2.25 (s, 3H), 1.59 (s, 3H). LC–MS (ESI): >95% purity at  $\lambda$  220 and 254 nm. MS:  $m/z$  181.1 [M + H]<sup>+</sup>.

**(2R)-2-Hydroxy-2,3-dimethylbenzeneacetic Acid Methyl Ester (24a, Y = H).** To a solution of (2R)-2-hydroxy-2,3-dimethylbenzeneacetic acid (23a, Y = H) (3.64 g, 20.2 mmol) in anhydrous diethyl ether (100 mL) was added diazomethane ether solution (freshly produced following procedures in Aldrich Technical Bulletin AL-180) until a bright yellow color is produced or no more bubbles evolved. The solution was then concentrated to dryness to obtain 3.9 g (99% yield) of a white solid. <sup>1</sup>H NMR (CDCl<sub>3</sub>, 500 MHz)  $\delta$ : 7.39 (s, 1H), 7.35 (d, 1H), 7.25 (t, 1H), 7.13 (d, 1H), 3.79 (s, 3H), 2.40 (s, 3H), 1.80 (s, 3H). LC–MS (ESI): >95% purity at  $\lambda$  220 and 254 nm. MS:  $m/z$  195.1 [M + H]<sup>+</sup>.

**(5R)-5-Methyl-5-(3-methylphenyl)-2,4-oxazolidinedione (25a, Y = H).** To a solution of methyl (2R)-2-hydroxy-2,3-dimethylbenzeneacetic acid methyl ester (24a, Y = H) (3.9 g, 20.1

mmol) in anhydrous ethanol (50 mL) were added NaOEt in ethanol (21 wt %/wt, 9.8 mL, 30 mmol), and urea (1.5 g, 24.2 mmol). The mixture was heated to 95 °C and refluxed overnight. The solution was then cooled to room temperature, acidified with 1 N HCl, concentrated to small volume, and diluted with water (100 mL). The aqueous mixture was extracted with ethyl acetate (3 × 50 mL). The organic extracts were combined, washed with brine, dried over anhydrous MgSO<sub>4</sub>, and concentrated to dryness to obtain 4.3 g (100% yield) of an oil which was used in the next step without further purification. <sup>1</sup>H NMR (CDCl<sub>3</sub>, 500 MHz) δ: 8.70 (s, broad, 1H), 7.4–7.2 (overlapping signals, 4H), 2.40 (s, 3H), 1.96 (s, 3H). MS: *m/z* 206.1 [M + H]<sup>+</sup>.

**(5R)-5-Methyl-5-(3-methylphenyl)-N-trityl-2,4-oxazolidinedione (26a, Y = H).** To a solution of (R)-5-methyl-5-(3-methylphenyl)oxazolidinedione (25a, 4.3 g, 20.9 mmol) in anhydrous methylene chloride (50 mL) were added triethylamine (2.1 g, 23 mmol) and trityl chloride (6.4 g, 23 mmol). The mixture was stirred under nitrogen at room temperature for 1 h, washed with water (20 mL), brine (20 mL), dried over anhydrous MgSO<sub>4</sub>, and concentrated to dryness to obtain 8.9 g (95% yield) of a solid. <sup>1</sup>H NMR (CDCl<sub>3</sub>, 500 MHz) δ: 7.40–7.20 (multiple overlapping peaks, 19H), 2.40 (s, 3H), 1.76 (s, 3H). MS: *m/z* 448.1 [M + H]<sup>+</sup>.

**(5R)-5-(3-Bromomethylphenyl)-5-methyl-N-trityl-2,4-oxazolidinedione (27a, Y = H).** To a solution of (R)-5-methyl-5-(3-methylphenyl)-N-trityloxazolidinedione (26a, 3.0 g, 6.7 mmol) in carbon tetrachloride (100 mL) were added N-bromosuccinimide (1.1 g, 6.7 mmol) and AIBN (catalytic). The mixture was heated to 80 °C and refluxed overnight. The solution was cooled to room temperature, washed with saturated NaHCO<sub>3</sub> solution (20 mL), water (20 mL), and brine (20 mL), and concentrated to dryness. The residue was purified by silica gel column chromatography with hexane/ethyl acetate (9:1) as a solvent to obtain 1.35 g (38% yield) of a white solid. <sup>1</sup>H NMR (CDCl<sub>3</sub>, 500 MHz) δ: 7.5–7.2 (multiple overlapping peaks, 19H), 4.56 (s, 2H), 1.76 (s, 3H). LC–MS (ESI): >95% purity at λ 220 and 254 nm. MS: *m/z* 526.1 [M + H]<sup>+</sup>. Enantiomeric purity: >96% ee.

For analysis of enantiomeric purities of the products, a 10 μL sample solution of approximately 1.0 mg/mL in concentration was injected onto a Chiralcel OD analytical column (4.6 mm × 50 mm, 10 μm). Products were then eluted with an isocratic solvent system consisting of 10% ethanol in heptane at a flow rate of 0.75 mL/min. Peaks were recorded at a wavelength of 220 μm with an UV detector. Under these conditions, the retention time of the S enantiomer is 6.96 min while the retention time of the R enantiomer is 8.98 min. Enantiomeric excess (% ee) is calculated as area under curve of the S enantiomer minus area under curve of the R enantiomer and divided by the sum of the two areas.

**General Procedures for Assembly of Most of the Final Target Compounds.** To a solution of intermediate 9 (0.1 mmol) in DMF (1 mL) were added the benzyl bromide intermediate such as 18 or 27 (0.1 mmol) and Cs<sub>2</sub>CO<sub>3</sub> (0.2 mmol). The mixture was stirred at room temperature overnight, diluted with water (1.0 mL), and extracted with ethyl acetate (2 × 1.0 mL). The organic extracts were combined, dried over anhydrous MgSO<sub>4</sub>, and concentrated to dryness to obtain a solid that was hydrolyzed either by NaOH in MeOH (in the case of 18) or by neat trifluoroacetic acid (in case of 27) followed by preparative HPLC purification to obtain final products. The following benzimidazolone analogues were prepared by this procedure unless described separately.

**(2R)-2-[2-Chloro-5-[3-(4-chlorobenzyl)-6-trifluoromethylbenzimidazol-1-yl]methyl]phenoxy]acetic Acid (28).** <sup>1</sup>H NMR (CDCl<sub>3</sub>, 500 MHz) δ: 7.28–7.34 (m, 5H), 7.13 (s, 1H), 6.99 (d, 1H), 6.94 (d, 1H), 6.88 (s, 1H), 6.85 (dd, 1H), 5.12 (dd, 2H), 5.06 (s, 2H), 4.78 (dd, 1H), 1.65 (d, 3H). LC–MS (ESI): >95% purity at λ 220 and 254 nm. MS: *m/z* 539.1 [M + H]<sup>+</sup>.

**(2R)-2-[2-Chloro-5-[3-(4-chlorobenzoyl)-6-trifluoromethylbenzimidazol-1-yl]methyl]phenoxy]acetic Acid (29).** <sup>1</sup>H NMR (CDCl<sub>3</sub>, 500 MHz) δ: 8.04 (d, 1H), 7.84 (dd, 2H), 7.57 (dd, 2H), 7.51 (m, 1H), 7.37 (m, 2H), 6.97 (m, 2H), 5.05 (dd, 2H), 4.97 (dd, 1H), 1.61 (d, 3H). LC–MS (ESI): >95% purity at λ 220 and 254 nm. MS: *m/z* 553.0 [M + H]<sup>+</sup>.

**(2R)-2-[2-Chloro-5-[3-(4-tert-butylphenyl)-6-trifluoromethylbenzimidazol-1-yl]methyl]phenoxy]acetic Acid (30).** <sup>1</sup>H NMR (CDCl<sub>3</sub>, 500 MHz) δ: 7.62 (m, 2H), 7.61 (s, 1H), 7.52 (d, 2H), 7.39 (m, 2H), 7.17 (d, 1H), 7.12 (s, 1H), 6.91 (d, 1H), 5.15 (dd, 2H), 4.77 (dd, 1H), 1.49 (d, 3H), 1.35 (s, 9H). LC–MS (ESI): >95% purity at λ 220 and 254 nm. MS: *m/z* 547.1 [M + H]<sup>+</sup>.

**(2R)-2-[2-Chloro-5-[3-(6-chlorobenzothiazol-2-yl)-6-trifluoromethylbenzimidazol-1-yl]methyl]phenoxy]acetic Acid (31).** <sup>1</sup>H NMR (CDCl<sub>3</sub>, 500 MHz) δ: 8.89 (d, 1H), 7.94 (d, 1H), 7.91 (s, 1H), 7.59 (d, 1H), 7.50 (dd, 1H), 7.40 (d, 1H), 7.23 (s, 1H), 7.01 (d, 1H), 6.91 (s, 1H), 5.12 (dd, 2H), 4.74 (dd, 1H), 1.67 (d, 3H). LC–MS (ESI): >95% purity at λ 220 and 254 nm. MS: *m/z* 582.0 [M + H]<sup>+</sup>.

**(2R)-2-[2-Chloro-5-[3-(6-chlorobenzisoxazol-3-yl)-6-trifluoromethylbenzimidazol-1-yl]methyl]phenoxy]acetic Acid (32).** <sup>1</sup>H NMR (CDCl<sub>3</sub>, 500 MHz) δ: 8.25 (d, 1H), 8.15 (s, 1H), 7.88 (d, 1H), 7.72 (s, 1H), 7.56 (d, 1H), 7.54 (d, 1H), 7.42 (d, 1H), 7.16 (s, 1H), 7.06 (d, 1H), 5.12 (s, 2H), 4.93 (dd, 1H), 1.50 (d, 3H). LC–MS (ESI): >95% purity at λ 220 and 254 nm. MS: *m/z* 566.1 [M + H]<sup>+</sup>.

**(2R)-2-[2-Chloro-5-[3-(7-methylbenzisoxazol-3-yl)-6-trifluoromethylbenzimidazol-1-yl]methyl]phenoxy]acetic Acid (33).** <sup>1</sup>H NMR (CDCl<sub>3</sub>, 500 MHz) δ: 8.09 (d, 1H), 7.90 (d, 1H), 7.58 (d, 1H), 7.43 (d, 1H), 7.39 (d, 1H), 7.25 (m, 2H), 6.98 (m, 2H), 5.19 (s, 2H), 4.78 (dd, 1H), 2.62 (s, 3H), 1.62 (d, 3H). LC–MS (ESI): >95% purity at λ 220 and 254 nm. MS: *m/z* 546.0 [M + H]<sup>+</sup>.

**(2R)-2-[2-Chloro-5-[3-(5-methylbenzisoxazol-3-yl)-6-trifluoromethylbenzimidazol-1-yl]methyl]phenoxy]acetic Acid (34).** <sup>1</sup>H NMR (CDCl<sub>3</sub>, 500 MHz) δ: 8.01 (d, 1H), 7.96 (d, 1H), 7.79 (d, 1H), 7.51 (m, 2H), 7.45 (t, 2H), 7.10 (d, 1H), 7.03 (d, 1H), 5.19 (dd, 2H), 4.80 (dd, 1H), 2.56 (s, 3H), 1.66 (d, 3H). LC–MS (ESI): >95% purity at λ 220 and 254 nm. MS: *m/z* 546.0 [M + H]<sup>+</sup>.

**(2R)-2-[2-Chloro-5-[3-(6-methylbenzisoxazol-3-yl)-6-trifluoromethylbenzimidazol-1-yl]methyl]phenoxy]acetic Acid (35).** <sup>1</sup>H NMR (CDCl<sub>3</sub>, 500 MHz) δ: 8.01 (m, 2H), 7.72 (m, 2H), 7.20 (m, 2H), 6.98 (m, 3H), 5.14 (s, 2H), 4.82 (m, 1H), 2.58 (s, 3H), 1.72 (d, 3H). LC–MS (ESI): >95% purity at λ 220 and 254 nm. MS: *m/z* 546.0 [M + H]<sup>+</sup>.

**(2R)-2-[2-Chloro-5-[3-(5-chlorobenzisoxazol-3-yl)-6-trifluoromethylbenzimidazol-1-yl]methyl]phenoxy]acetic Acid (36).** <sup>1</sup>H NMR (CDCl<sub>3</sub>, 500 MHz) δ: 8.30 (d, 1H), 8.14 (s, 1H), 7.99 (s, 1H), 7.60 (d, 1H), 7.54 (d, 1H), 7.45 (d, 1H), 7.39 (d, 1H), 7.16 (s, 1H), 7.02 (d, 1H), 5.17 (dd, 2H), 4.91 (m, 1H), 1.50 (d, 3H). LC–MS (ESI): >95% purity at λ 220 and 254 nm. MS: *m/z* 566.1 [M + H]<sup>+</sup>.

**(2R)- and (2S)-2-[2-Chloro-5-[3-(6-methoxybenzisoxazol-3-yl)-6-trifluoromethylbenzimidazol-1-yl]methyl]phenoxy]acetic Acid (37 and 41).** <sup>1</sup>H NMR (CDCl<sub>3</sub>, 500 MHz) δ: 8.07 (d, 1H), 7.95 (d, 1H), 7.50 (d, 1H), 7.42 (d, 1H), 7.28 (s, 1H), 7.01–7.08 (m, 4H), 5.15 (dd, 2H), 4.79 (dd, 1H), 3.96 (s, 3H), 1.71 (d, 3H). LC–MS (ESI): >95% purity at λ 220 and 254 nm. MS: *m/z* 562.0 [M + H]<sup>+</sup>.

**(2R)-2-[2-Chloro-5-[3-(6-methoxybenzisoxazol-3-yl)-6-trifluoromethoxybenzimidazol-1-yl]methyl]phenoxy]acetic Acid (38).** <sup>1</sup>H NMR (CDCl<sub>3</sub>, 500 MHz) δ: 8.13 (d, 1H), 7.76 (s, 1H), 7.32 (d, 1H), 7.23 (s, 3H), 7.10 (s, 1H), 7.03 (t, 2H), 5.27 (dd, 2H), 4.45 (m, 1H), 3.95 (s, 3H), 1.57 (d, 3H). LC–MS (ESI): >95% purity at λ 220 and 254 nm. MS: *m/z* 578.0 [M + H]<sup>+</sup>.

**(2R)-2-[2-Chloro-5-[3-(6-methoxybenzisoxazol-3-yl)-5-trifluoromethylbenzimidazol-1-yl]methyl]phenoxy]acetic Acid (39).** <sup>1</sup>H NMR (CDCl<sub>3</sub>, 500 MHz) δ: 8.09 (d, 1H), 7.85 (s, 1H), 7.47 (d, 1H), 7.38 (m, 3H), 7.26 (s, 1H), 7.5 (t, 2H), 5.16 (dd, 2H), 4.81 (m, 1H), 3.96 (s, 3H), 1.68 (d, 3H). LC–MS (ESI): >95% purity at λ 220 and 254 nm. MS: *m/z* 562.0 [M + H]<sup>+</sup>.

**(2R)-2-[2-Chloro-5-[3-(6-methoxybenzisoxazol-3-yl)-5-trifluoromethoxybenzimidazol-1-yl]methyl]phenoxy]acetic Acid (40).** <sup>1</sup>H NMR (CDCl<sub>3</sub>, 500 MHz) δ: 8.13 (d, 1H), 7.75 (s, 1H), 7.37 (d, 1H), 7.13 (m, 3H), 7.06 (s, 1H), 7.01 (t, 2H), 5.16 (dd, 2H), 4.82 (m, 1H), 3.94 (s, 3H), 1.61 (d, 3H). LC–MS (ESI): >95% purity at λ 220 and 254 nm. MS: *m/z* 578.0 [M + H]<sup>+</sup>.

**(2R)-2-[4-Chloro-3-[3-(6-methoxybenzisoxazol-3-yl)-6-trifluoromethylbenzimidazol-1-yl]methyl]phenoxy]acetic Acid**

(42).  $^1\text{H}$  NMR ( $\text{CDCl}_3$ , 500 MHz)  $\delta$ : 8.26 (d, 1H), 7.97 (d, 1H), 7.82 (s, 1H), 7.51 (d, 1H), 7.44 (d, 1H), 7.40 (s, 1H), 7.38 (m, 1H), 6.87 (m, 2H), 5.31 (s, 2H), 4.73 (dd, 1H), 3.94 (s, 3H), 1.49 (d, 3H). LC–MS (ESI): >95% purity at  $\lambda$  220 and 254 nm. MS:  $m/z$  562.0  $[\text{M} + \text{H}]^+$ .

(2R)-2-[3-[3-(6-Methoxybenzisoxazol-3-yl)-6-trifluoromethylbenzimidazol-1-yl]methyl]phenoxy]acetic Acid (43).  $^1\text{H}$  NMR ( $\text{CDCl}_3$ , 500 MHz)  $\delta$ : 8.25 (d, 1H), 8.15 (s, 1H), 7.89 (d, 1H), 7.70 (s, 1H), 7.56 (t, 2H), 7.27 (t, 1H), 7.04 (d, 1H), 6.96 (s, 1H), 6.78 (d, 1H), 5.23 (s, 2H), 4.80 (dd, 1H), 3.98 (s, 3H), 1.46 (d, 3H). LC–MS (ESI): >95% purity at  $\lambda$  220 and 254 nm. MS:  $m/z$  528.1  $[\text{M} + \text{H}]^+$ .

(2R)-2-[3-[3-(6-Methoxybenzisoxazol-3-yl)-6-trifluoromethylbenzimidazol-1-yl]methyl]phenoxy]propanoic Acid (44).  $^1\text{H}$  NMR ( $\text{CDCl}_3$ , 500 MHz)  $\delta$ : 8.25 (d, 1H), 8.15 (s, 1H), 7.88 (d, 1H), 7.72 (s, 1H), 7.55 (t, 2H), 7.26 (t, 1H), 7.01 (s, 2H), 6.79 (d, 1H), 5.22 (s, 2H), 4.63 (m, 1H), 3.92 (s, 3H), 1.85 (m, 2H), 0.95 (t, 3H). LC–MS (ESI): >95% purity at  $\lambda$  220 and 254 nm. MS:  $m/z$  541.1  $[\text{M} + \text{H}]^+$ .

(5R)-5-(2-[3-(6-Methoxy-1,2-benzisoxazol-3-yl)-6-trifluoromethylbenzimidazol-1-yl]methyl]phenyl)-5-methyloxazolidinedione (45).  $^1\text{H}$  NMR ( $\text{CDCl}_3$ , 500 MHz)  $\delta$ : 8.12 (d, 1H), 8.01 (d, 1H), 7.62 (s, 1H), 7.50 (s, 1H), 7.40–7.49 (m, 3H), 7.23 (s, 1H), 7.10 (s, 1H), 7.05 (d, 1H), 5.20 (s, 2H), 3.96 (s, 3H), 1.98 (s, 3H). LC–MS (ESI): >95% purity at  $\lambda$  220 and 254 nm. MS:  $m/z$  553.1  $[\text{M} + \text{H}]^+$ .

(5R)-5-(4-[3-(6-Methoxy-1,2-benzisoxazol-3-yl)-6-trifluoromethylbenzimidazol-1-yl]methyl]phenyl)-5-methyloxazolidinedione (46).  $^1\text{H}$  NMR ( $\text{CDCl}_3$ , 500 MHz)  $\delta$ : 8.19 (d, 1H), 7.98 (d, 1H), 7.65 (d, 2H), 7.52 (d, 2H), 7.13 (d, 1H), 7.11 (s, 1H), 7.02 (d, 1H), 6.83 (s, 1H), 5.20 (s, 2H), 3.98 (s, 3H), 1.99 (s, 3H). LC–MS (ESI): >95% purity at  $\lambda$  220 and 254 nm. MS:  $m/z$  553.1  $[\text{M} + \text{H}]^+$ .

(5R)-5-(3-[3-(6-Methoxy-1,2-benzisoxazol-3-yl)-6-trifluoromethylbenzimidazol-1-yl]methyl]phenyl)-5-methyloxazolidinedione (47).  $^1\text{H}$  NMR ( $\text{CDCl}_3$ , 500 MHz)  $\delta$ : 8.14 (d, 1H), 8.01 (d, 1H), 7.72 (s, 1H), 7.58 (s, 1H), 7.40–7.49 (m, 3H), 7.21 (s, 1H), 7.07 (s, 1H), 7.03 (d, 1H), 5.25 (s, 2H), 3.96 (s, 3H), 1.96 (s, 3H). LC–MS (ESI): >95% purity at  $\lambda$  220 and 254 nm. MS:  $m/z$  553.1  $[\text{M} + \text{H}]^+$ .

(5R)-5-(3-[3-(6-Methoxy-1,2-benzisoxazol-3-yl)-6-trifluoromethylbenzimidazol-1-yl]phenyl)-5-methyloxazolidinedione (48).  $^1\text{H}$  NMR ( $\text{CDCl}_3$ , 500 MHz)  $\delta$ : 8.18 (d, 1H), 8.05 (d, 1H), 7.70 (s, 1H), 7.62 (s, 1H), 7.38–7.52 (m, 3H), 7.25 (s, 1H), 7.17 (s, 1H), 7.05 (d, 1H), 3.98 (s, 3H), 1.98 (s, 3H). LC–MS (ESI): >95% purity at  $\lambda$  220 and 254 nm. MS:  $m/z$  539.0  $[\text{M} + \text{H}]^+$ .

(5R)-5-(3-[3-(6-Methoxy-1,2-benzisoxazol-3-yl)-6-trifluoromethylbenzimidazol-1-yl]methyl]-4-chlorophenyl)-5-methyloxazolidinedione (49).  $^1\text{H}$  NMR ( $\text{CDCl}_3$ , 500 MHz)  $\delta$ : 8.14 (d, 1H), 8.02 (d, 1H), 7.67 (s, 1H), 7.57 (s, 1H), 7.52 (d, 1H), 7.26 (m, 2H), 7.09 (s, 1H), 7.06 (d, 1H), 5.38 (s, 2H), 3.98 (s, 3H), 1.83 (s, 3H). LC–MS (ESI): >95% purity at  $\lambda$  220 and 254 nm. MS:  $m/z$  587.0  $[\text{M} + \text{H}]^+$ .

(2R)-2-[2-Chloro-5-[3-(6-methoxybenzisoxazol-3-yl)-benzimidazol-1-yl]methyl]phenoxy]acetic Acid (50).  $^1\text{H}$  NMR ( $\text{CDCl}_3$ , 500 MHz)  $\delta$ : 8.13 (d, 1H), 7.88 (dd, 1H), 7.37 (d, 1H), 7.25 (m, 2H), 7.08 (d, 1H), 7.02 (dd, 2H), 6.98 (dd, 1H), 6.77 (s, 1H), 5.29 (d, 2H), 4.64 (dd, 1H), 3.97 (s, 3H), 1.59 (d, 3H). LC–MS (ESI): >95% purity at  $\lambda$  220 and 254 nm. MS:  $m/z$  494.1  $[\text{M} + \text{H}]^+$ .

(5R)-5-(3-[3-(6-Methoxybenzisoxazol-3-yl)benzimidazol-1-yl]methyl]phenyl)-5-methyloxazolidinedione (51). To a solution of 1-[3-(6-methoxy)-benzisoxazolyl]benzimidazole-2-one (9j, 266 mg, 0.95 mmol) in DMF (3 mL) were added (R)-5-methyl-5-(3-bromomethylphenyl)-N-trityloxazolidinedione (27a, 500 mg, 0.95 mmol) and  $\text{Cs}_2\text{CO}_3$  (620 mg, 1.9 mmol). The mixture was stirred at room temperature overnight, diluted with water (10 mL), and extracted with ethyl acetate ( $2 \times 10$  mL). The organic extracts were combined, dried over anhydrous  $\text{MgSO}_4$ , and concentrated to obtain a solid. The solid was dissolved in neat TFA (5 mL), and the mixture was stirred at room temperature for 6 h. The mixture was then concentrated to dryness under vacuum and purified by silica gel column chromatography with hexane/ethyl acetate/TFA (3/1/0.01)

as solvent system to obtain 358 mg (78% yield) of a white solid.  $^1\text{H}$  NMR (500 MHz,  $\text{CDCl}_3$ )  $\delta$ : 8.18 (d, 1H), 7.92 (d, 1H), 7.71 (s, 1H), 7.56 (brs, 1H), 7.43 (brs, 2H), 7.23 (m, 2H), 7.08 (s, 1H), 7.02 (m, 2H), 5.28 (dd, 2H), 3.98 (s, 3H), 1.99 (s, 3H). LC–MS (ESI): >95% purity at  $\lambda$  220 and 254 nm. MS:  $m/z$  485.1  $[\text{M} + \text{H}]^+$ . Enantiomeric purity: >96% ee. Enantiomeric purities of the product were determined by chiral HPLC on a Chiralcel OD analytical column (4.6 mm  $\times$  50 mm, 10  $\mu\text{m}$ ). The product was eluted with an isocratic solvent system consisting of 10% ethanol in heptane at a flow rate of 0.75 mL/min. Under these conditions, the retention time of the S enantiomer is approximately 14 min while the retention time of the R enantiomer is about 17 min. Enantiomeric purity for other analogues should be similar, since their chiralities were derived from the same intermediate (27a).

(5R)-5-(3-[3-(6-Chlorobenzisoxazol-3-yl)benzimidazol-1-yl]methyl]phenyl)-5-methyloxazolidinedione (52).  $^1\text{H}$  NMR ( $\text{CDCl}_3$ , 500 MHz)  $\delta$ : 8.39 (s, 1H), 8.33 (brs, 1H), 7.92 (d, 1H), 7.71 (s, 1H), 7.61 (s, 2H), 7.58 (d, 1H), 7.42 (m, 2H), 7.21 (d, 2H), 7.02 (d, 1H), 5.23 (dd, 2H), 1.99 (s, 3H). LC–MS (ESI): >95% purity at  $\lambda$  220 and 254 nm. MS:  $m/z$  489.0  $[\text{M} + \text{H}]^+$ .

(2R)-2-[4-Chloro-3-[3-(6-methoxybenzisoxazol-3-yl)-benzimidazol-1-yl]methyl]phenoxy]acetic Acid (53).  $^1\text{H}$  NMR ( $\text{CDCl}_3$ , 500 MHz)  $\delta$ : 8.12 (d, 1H), 7.98 (dd, 1H), 7.37 (d, 1H), 7.15 (m, 2H), 7.12 (d, 1H), 7.05 (dd, 2H), 6.78 (dd, 1H), 6.87 (s, 1H), 5.29 (d, 2H), 4.64 (dd, 1H), 3.97 (s, 3H), 1.59 (d, 3H). LC–MS (ESI): >95% purity at  $\lambda$  220 and 254 nm. MS:  $m/z$  494.1  $[\text{M} + \text{H}]^+$ .

(5R)-5-(3-[3-(6-Methoxy-1,2-benzisoxazol-3-yl)benzimidazol-1-yl]methyl)-4-chlorophenyl)-5-methyloxazolidinedione (54).  $^1\text{H}$  NMR ( $\text{CDCl}_3$ , 500 MHz)  $\delta$ : 8.18 (d, 1H), 7.93 (d, 1H), 7.60 (s, 1H), 7.58 (s, 1H), 7.23 (m, 2H), 7.08 (m, 4H), 5.26 (s, 2H), 3.94 (s, 3H), 1.86 (s, 3H). LC–MS (ESI): >95% purity at  $\lambda$  220 and 254 nm. MS:  $m/z$  519.1  $[\text{M} + \text{H}]^+$ .

## ■ ASSOCIATED CONTENT

### Supporting Information

Additional experimental procedures for synthesis of 4–7 and 11–18, elemental analysis results for 51 and 52, structures and spectra data of other benzimidazolones analogues, and chiral HPLC traces of selected compounds. This material is available free of charge via the Internet at <http://pubs.acs.org>.

### Accession Codes

$\dagger$ Protein Data Bank (PDB) access code for X-ray crystallographic data of compound 51: 3TY0.

## ■ AUTHOR INFORMATION

### Corresponding Author

\*Phone: 732-594-2782. Fax: 732-594-9556. E-mail: [weiguo\\_liu@merck.com](mailto:weiguo_liu@merck.com).

## ■ ACKNOWLEDGMENTS

We gratefully acknowledge the technical assistance from Neelam Sharma and Roger Meurer. We also thank Dr. Stephen Soisson for depositing the X-ray coordinates and Dr. Gino Salituro for PK studies.

## ■ ABBREVIATIONS USED

T2DM, type 2 diabetes mellitus; PPAR, peroxisome proliferator-activated receptor; SPPAR $\gamma$ M, selective peroxisome proliferator-activated receptor  $\gamma$  modulator; CYP, cytochrome P450; TZD, thiazolidinedione; PV, plasma volume; mpk, mg/kg

## ■ REFERENCES

(1) Albrecht, S. S.; Kuklina, E. V.; Bansil, P.; Jamieson, D. J.; Whiteman, M. K.; Kourtis, A. P.; Posner, S. F.; Callaghan, W.

Diabetes: trends among delivery hospitalizations in the U.S., 1994–2004. *Diabetes Care* **2010**, *33*, 768–773.

(2) Willson, T. M.; Brown, P. J.; Sternbach, D. D.; Henke, B. R. The PPARs: from orphan receptor to drug discovery. *J. Med. Chem.* **2000**, *43*, 527–550.

(3) Kersten, S.; Desvergne, B.; Wahli, W. Roles of PPARs in health and disease. *Nature* **2000**, *405*, 421–424.

(4) Nuclear Receptors Nomenclature Committee, 1999. A unified nomenclature system for the nuclear receptor superfamily. *Cell* **1999**, *97*, 161–163.

(5) Berger, J.; Bailey, P.; Biswas, C.; Cullinan, C. A.; Doebber, T. W.; Hayes, N. S.; Saperstein, R.; Smith, R. G.; Leibowitz, M. D. Thiazolidinediones produce a conformational change in peroxisomal proliferator-activated receptor- $\gamma$ : binding and activation correlates with antidiabetic actions in db/db mice. *Endocrinology* **1996**, *137*, 4189–4195.

(6) Oakes, N. D.; Kennedy, C. J.; Jenkins, A. B.; Laybutt, D. R.; Chisholm, D. J.; Kraegen, E. W. A new anti-diabetic agent, BRL 49653, reduces lipid availability and improves insulin action and glucose regulation in the rat. *Diabetes* **1994**, *43*, 1203–1210.

(7) Nesto, R. W.; Bell, D.; Bonow, R. O.; Fonseca, V.; Grundy, S. M.; Horton, E. S.; Winter, M. L.; Porte, D.; Semenkovich, C. F.; Smith, S.; Young, L. H.; Kahn, R. Thiazolidinedione use, fluid retention, and congestive heart failure: a consensus statement from the American Heart Association and American Diabetes Association. *Diabetes Care* **2004**, *27*, 256–263.

(8) Kahn, S. E.; Zinman, B.; Lachin, J. M.; Haffner, S. M.; Herman, W. H.; Holman, R. R.; Kravitz, B. G.; Yu, D.; Heise, M. A.; Aftring, R. P.; Viberti, G. Rosiglitazone-associated fractures in type 2 diabetes: an analysis from A Diabetes Outcome Progression Trial (ADOPT). *Diabetes Care* **2008**, *31*, 845–851.

(9) Burgermeister, E.; Schnoebelen, A.; Flament, A.; Benz, J.; Stihle, M.; Gsell, B.; Rufer, A.; Kuhn, B.; Marki, H. P. A novel partial agonist of peroxisomal proliferator-activated receptor- $\gamma$  (PPAR $\gamma$ ) recruits PPAR $\gamma$ -coactivator-1 $\alpha$ , prevents triglyceride accumulation, and potentiates insulin signaling in vitro. *Mol. Endocrinol.* **2006**, *20*, 809–830.

(10) (a) Berger, J. P.; Petro, A. E.; McNaul, K. L.; Kelly, L. J.; Zhang, B. B.; Richards, K.; Elbrecht, A.; Johnson, B. A.; Zhou, G.; Doebber, T. W.; Biswas, C.; Parikh, M.; Sharma, N.; Tanen, M. R.; Thompson, G. M.; Ventre, J.; Adams, A. D.; Mosley, R.; Surwit, R. S.; Moller, D. E. Distinct properties and advantages of a novel peroxisomal proliferator-activated protein- $\gamma$  selective modulator. *Mol. Endocrinol.* **2003**, *17*, 662–676. (b) Meinke, P. T.; Wood, H. B.; Szewczyk, J. W. Nuclear hormone receptor modulators for the treatment of diabetes and dyslipidemia. *Annu. Rep. Med. Chem.* **2006**, *41*, 99–126.

(11) Elbrecht, A.; Chen, Y.; Adams, A.; Berger, J. P.; Griffin, P.; Klatt, T.; Zhang, B. B.; Menke, J.; Zhou, G.; Smith, R. G.; Moller, D. E. L-764406 is a partial agonist of human peroxisomal proliferator-activated receptor- $\gamma$ . The role of CYS313 in ligand binding. *J. Biol. Chem.* **1999**, *274*, 7913–7922.

(12) (a) Acton, J. J.; Black, R. M.; Jones, A. B.; Moller, D. E.; Colwell, L.; Doebber, T. W.; MacNaul, K. L.; Berger, J.; Wood, H. B. Benzoyl 2-methyl indoles as selective PPAR $\gamma$  modulators. *Bioorg. Med. Chem. Lett.* **2005**, *15*, 357–362. (b) Liu, K.; Black, R. M.; Acton, J. A. III; Mosley, R.; Debenham, S.; Abola, R.; Yang, M.; Tschirret-Guth, R.; Colwell, L.; Liu, C.; Wu, M.; Wang, C. F.; MacNaul, K. L.; McCann, M. E.; Moller, D. E.; Berger, J. P.; Meinke, P. T.; Jones, A. B.; Wood, H. B. Selective PPAR $\gamma$  modulators with improved pharmacological profiles. *Bioorg. Med. Chem. Lett.* **2005**, *15*, 2437–2440. (c) Liu, W.; Liu, K.; Wood, H. B.; McCann, M. E.; Doebber, T. W.; Chang, C. H.; Akiyama, T. E.; Einstein, M.; Berger, J. P.; Meinke, P. T. Discovery of a peroxisomal proliferator activated receptor  $\gamma$  (PPAR $\gamma$ ) modulator with balanced PPAR $\alpha$  activity for the treatment of type 2 diabetes and dyslipidemia. *J. Med. Chem.* **2009**, *52*, 4443–4453. (d) Acton, J. J. III; Akiyama, T. E.; Chang, C. H.; Colwell, L.; Debenham, S.; Doebber, T.; Einstein, M.; Liu, K.; McCann, M. E.; Moller, D. E.; Muise, E. S.; Tan, Y.; Thompson, J. R.; Wong, K. K.; Wu, M.; Xu, L.; Meinke, P. T.; Berger, J. P.; Wood, H. B. *J. Med. Chem.* **2009**, *52*, 3846–3854.

(13) Debenham, S. D.; Chan, A.; Lau, F. W.; Liu, W.; Wood, H. B.; Lemme, K.; Colwell, L.; Habulihaz, B.; Akiyama, T. E.; Einstein, M.; Doebber, T. W.; Sharma, N.; Wang, C. F.; Wu, M.; Berger, J. P.; Meinke, P. T. Highly functionalized 7-azaindoles as selective PPAR $\gamma$  modulators. *Bioorg. Med. Chem. Lett.* **2008**, *18*, 4798–4801.

(14) Geffken, D. Cyclization of salicylamides and salicylohydroxamic acids with 1,1'-carbonyldiimidazole. *Liebigs Ann. Chem.* **1981**, 1513–1514.

(15) McConville, M.; Blacker, J.; Xiao, J. Heck reaction in diols and cascade formation of cyclic ketals. *Synthesis* **2010**, 349–360.

(16) Wang, Z.-M.; Sharpless, K. B. A solid to solid asymmetric dihydroxylation procedure for kilogram-scale preparation of enantiopure hydrobenzoin. *J. Org. Chem.* **1994**, *59*, 8302–8303.

(17) For the binding assay procedure, see the following: Adams, A. D.; Yuen, W.; Hu, Z.; Santini, C.; Jones, A. B.; MacNaul, K. L.; Berger, J. P.; Doebber, T. W.; Moller, D. E. Amphipathic 3-phenyl-7-propylbenzoxazoles; human PPAR $\gamma$ ,  $\delta$  and  $\alpha$  agonists. *Bioorg. Med. Chem. Lett.* **2003**, *13*, 931–936.

(18) Berger, J. B.; Bailey, P.; Biswas, C.; Cillina, C. A.; Doebber, T. W.; Hayes, N. S.; Saperstein, R.; Smith, R. G.; Leibowitz, M. D. Thiazolidinediones produce a conformational change in peroxisomal proliferator-activated receptor-gamma: binding and activation correlate with antidiabetic actions in db/db mice. *Endocrinology* **1996**, *137*, 4189–4195.

(19) Gani, O. A. B. S. M.; Sylte, I. Ligand-induced stabilization and activation of peroxisomal proliferator-activated receptor  $\gamma$ . *Chem. Biol. Drug Des.* **2008**, *72*, 50–57.

(20) Einstein, M.; Akiyama, T. E.; Castriota, G. A.; Wang, C. F.; McKeever, B.; Mosley, R. T.; Becker, J. W.; Moller, D. E.; Meinke, P. T.; Wood, H. B.; Berger, J. P. The differential interactions of peroxisomal proliferator-activator receptor  $\gamma$  ligands with Tyr473 is a physical basis for their unique biological activities. *Mol. Pharmacol.* **2008**, *73*, 62–74.

(21) Lamotte, Y.; Martres, P.; Faucher, N.; Laroze, A.; Grillot, D.; Ancellin, N.; Saintillan, Y.; Beneton, V.; Gampe, R. T. Jr. Synthesis and biological activities of novel indole derivatives as potent and selective PPAR $\gamma$  modulators. *Bioorg. Med. Chem. Lett.* **2010**, *20*, 1399–1404.

(22) Nolte, R. T.; Wisely, G. B.; Westin, S.; Cobb, J. E.; Lambert, M. H.; Kurokawa, R.; Rosenfeld, M. G.; Willson, T. M.; Glass, C. K.; Milburn, M. V. Ligand binding and co-activator assembly of the peroxisomal proliferator-activated receptor-gamma. *Nature* **1998**, *395*, 137–143.

(23) Sheu, S. H.; Kaya, T.; Waxman, D. J.; Vajda, S. Exploring the binding site structure of the PPAR gamma ligand-binding domain by computational solvent mapping. *Biochemistry* **2005**, *44*, 1193–1209.

(24) Schupp, M.; Clemenz, M.; Gineste, R.; Witt, H.; Janke, J.; Helleboid, S.; Hennuyer, N.; Ruiz, P.; Unger, T.; Staels, B.; Kintscher, U. Molecular characterization of new selective peroxisomal proliferator-activated receptor gamma modulators with angiotensin receptor blocking activity. *Diabetes* **2005**, *54*, 3442–3452.

(25) Thieme, T. M.; Steri, R.; Proschak, E.; Paulke, A.; Schneider, G.; Schubert-Zsilavecz, M. Rational design of a piriinic acid derivative that acts as subtype-selective PPAR $\gamma$  modulator. *Bioorg. Med. Chem. Lett.* **2010**, *20*, 2469–2473.

(26) Furukawa, A.; Arita, T.; Satoh, S.; Wakabayashi, K.; Hayashi, S.; Matsui, Y.; Araki, K.; Kuroha, M.; Ohsumi, J. Discovery of a novel selective PPAR $\gamma$  modulator from (–)-cercosporamide derivatives. *Bioorg. Med. Chem. Lett.* **2010**, *20*, 2095–2098.

(27) McKenna, N. J.; O'Malley, B. W. Minireview: nuclear receptor coactivators—an update. *Endocrinology* **2002**, *143*, 2461–2465.

(28) Dreijerink, K. M. A.; Varier, R. A.; van Beekum, O.; Jenning, E. H.; Hoeppener, J. W. M.; Lips, C. J. M.; Kummer, J. A.; Kalkhoven, E.; Timmers, H. T. M. The multiple endocrine neoplasia type 1 (MEN1) tumor suppressor regulates peroxisomal proliferator-activated receptor  $\gamma$ -dependent adipocyte differentiation. *Mol. Cell. Biol.* **2009**, *29*, S060–S069.

(29) Pochetti, G.; Mitro, N.; Lavecchia, A.; Gilardi, F.; Besker, N.; Scotti, E.; Aschi, M.; Re, N.; Fracchiolla, G.; Laghezza, A.; Tortorella, P.; Montanari, R.; Novellino, E.; Mazza, F.; Crestani, M.; Loidice, F.

Structural insight into peroxisome proliferator-activated receptor  $\gamma$  binding of two ureidofibrate-like enantiomers by molecular dynamics, cofactor interaction analysis, and site-directed mutagenesis. *J. Med. Chem.* **2010**, *53*, 4354–4366.

(30) Zhou, G.; Cummings, R.; Hermes, J.; Moller, D. E. Use of homogeneous time-resolved fluorescence energy transfer in the measurement of nuclear receptor activation. *Methods* **2001**, *26*, 54–61.

(31) Torchia, J.; Rose, D. W.; Inostroza, J.; Kamei, Y.; Westin, S.; Glass, C. K.; Rosenfeld, M. G. The transcriptional co-activator p/CIP binds CBP and mediates nuclear-receptor function. *Nature* **1997**, *387*, 677–684.

(32) Sadana, P.; Park, E. A. Characterization of the transactivation domain in the peroxisome-proliferator-activated receptor  $\gamma$  co-activator (PGC-1). *Biochem. J.* **2007**, *403*, 511–518.

(33) Leo, C.; Chen, J. D. The SRC family of nuclear receptor coactivators. *Gene* **2000**, *245*, 1–11.

(34) Zhu, Y.; Qi, C.; Jain, S.; Rao, M. S.; Reddy, J. K. Isolation and characterization of PBP, a protein that interacts with peroxisome proliferator-activated receptor. *J. Biol. Chem.* **1997**, *272*, 25500–25506.

(35) Li, Y.; Kovach, A.; Suino-Powell, K.; Martynowski, D.; Xu, H. E. Structural and biochemical basis for the binding selectivity of peroxisome proliferator-activated receptor  $\gamma$  to PGC-1.alpha. *J. Biol. Chem.* **2008**, *283*, 19132–19139.

(36) Burgermeister, E.; Schnoebelen, A.; Flament, A.; Benz, J.; Stihle, M.; Gsell, B.; Rifer, A.; Ruf, A.; Kuhn, B.; Marki, H. P.; Mizrahi, J.; Sebokova, E.; Niesor, E.; Meyer, M. A novel partial agonist of peroxisome proliferator activated receptor- $\gamma$  (PPAR $\gamma$ ) recruits PPAR $\gamma$ -coactivator-1a, prevents triglyceride accumulation, and potentiates insulin signaling in vitro. *Mol. Endocrinol.* **2006**, *20*, 809–830.

(37) Sorbera, L. A.; Leeson, P. A.; Martin, L.; Castaner, J. Farglitazar. Antidiabetic PPAR $\gamma$  agonist. *Drugs Future* **2001**, *26*, 354–363.

(38) White, I. R.; Man, W. J.; Bryant, D.; Bugelski, P.; Camilleri, P.; Cutler, P.; Hayes, W.; Holbrook, J. D.; Kramer, K.; Lord, P. G.; Wood, J. Protein expression changes in the Sprague Dawley rat liver proteome following administration of peroxisome proliferator activated receptor alpha and gamma ligands. *Proteomics* **2003**, *3*, 505–512.

(39) Berger, J.; Leibowitz, M. D.; Doebber, T. W.; Elbrecht, A.; Zhang, B.; Zhou, G.; Biswas, C.; Cullinan, C. A.; Hayes, N. S.; Li, Y.; Tanen, M.; Ventre, J.; Wu, M. S.; Berger, G. D.; Mosley, R.; Marquis, R.; Santini, C.; Sahoo, S. P.; Tolman, R. L.; Smith, R. G.; Moller, D. E. Novel peroxisome proliferator-activated receptor (PPAR)  $\gamma$  and PPAR $\delta$  ligands produce distinct biological effects. *J. Biol. Chem.* **1999**, *274*, 6718–6725.

(40) Chang, C. H.; McNamara, L. A.; Wu, M. S.; Muise, E. S.; Tan, Y.; Wood, H. B.; Meinke, P. T.; Thompson, J. R.; Doebber, T. W.; Berger, J. P.; McCann, M. E. A novel selective peroxisome proliferator-activator receptor-gamma modulator-SPPAR $\gamma$ MS improves insulin sensitivity with diminished adverse cardiovascular effects. *Eur. J. Pharmacol.* **2008**, *584*, 192–201.